A&A 423, 1029–1044 (2004)
DOI: 10.1051/0004-6361:20040202

Astronomy & Astrophysics

XMM-Newton probes the stellar population in Chamaeleon I South⋆

B. Stelzer[1], G. Micela[1], and R. Neuhäuser[2]

[1] INAF - Osservatorio Astronomico di Palermo, Piazza del Parlamento 1, 90134 Palermo, Italy
e-mail: stelzer@astropa.unipa.it
[2] Astrophysikalisches Institut und Universitäts-Sternwarte, Schillergässchen 2-3, 07745 Jena, Germany

Received 5 February 2004 / Accepted 31 March 2004

Abstract. We report on a 30 ks *XMM-Newton* observation of the central region of the Cha I star forming cloud. The field includes a substantial fraction of the known pre-main-sequence population of Cha I South, including all thirteen known very-low mass Hα emitters. We detect two bona-fide brown dwarfs (spectral types M 7.5 and M 8) and seven Hα emitting objects near the hydrogen burning mass limit, including six of seven earlier detections by *ROSAT*. Three objects classified as Cha I candidate members according to their NIR photometry are revealed by *XMM-Newton*, providing further evidence for them being truly young stars. A total of 11 new X-ray sources without known optical/IR counterpart may comprise further as yet unrecognized faint cloud members. Spectral analysis of the X-ray bright stars shows that previous X-ray studies in Cha I have underestimated the X-ray luminosities, as a result of simplified assumptions on the spectral shape. In particular, the extinction is variable over the field, such that the choice of a uniform value for the column density is inappropriate. We establish that the X-ray saturation level for the late-type stars in Cha I is located near $L_{\rm x}/L_{\rm bol} \sim 10^{-2.5}$, with a possible decline to $L_{\rm x}/L_{\rm bol} \sim 10^{-3}$ for the lowest mass stars. A group of strongly absorbed stars with unusually hard X-ray emission is clustered around HD 97048, a HAeBe star and the only confirmed intermediate-mass star in the field. While the X-ray properties of HD 97048 are indistinguishable from those of its lower-mass neighbors, another presumably A-type star (identified as such based on NIR photometry) stands out as the softest X-ray emitter in the whole sample. This suggests that various X-ray emission mechanisms may be at work in intermediate-mass pre-main-sequence stars. We find that X-ray luminosity follows a tight correlation with age, effective temperature, and mass. No dramatic changes in these correlations are seen at the substellar boundary, suggesting that the same dynamo mechanism operates in both low-mass stars and brown dwarfs, at least at young ages. The variability of the lowest-mass objects is also similar to that of higher-mass T Tauri stars. X-ray flares are seen in about 1/10th of the Cha I members in the field.

Key words. X-rays: stars – stars: pre-main-sequence – stars: low-mass, brown dwarfs – stars: coronae – stars: activity

1. Introduction

The Chamaeleon cloud complex is one of the most nearby star forming complexes, composed of three major clouds. Their isolated position at high galactic latitude ($b \approx -15°$), resulting in both low foreground extinction and low contamination with background objects, makes them attractive targets for the study of the formation of low-mass stars.

Cha I hosts the largest number of known low-mass pre-main-sequence (PMS) stars and is one of the best-studied of these regions (see e.g., Schwartz 1977; Gauvin & Strom 1992; Prusti et al. 1992; Hartigan 1993). A substantial number of the Cha I cloud members have first been identified as X-ray sources in pointed *ROSAT* observations (Feigelson et al. 1993, henceforth F93), and have later – with the help of optical observations – been confirmed as PMS stars (Lawson et al. 1996, henceforth LFH96). In contrast to most of the previously known Cha I members, the so-called classical T Tauri stars (cTTS), they belong to the class of weak-line T Tauri stars (wTTS), i.e. they show only weak Hα emission, presumably because accretion has ceased after the dispersal of the circumstellar disk. LFH96 estimate that the number ratio of wTTS to cTTS in Cha I is $\geq$2. Both populations of TTS stars are mixed in the Hertzsprung-Russell diagram (HRD), indicating a wide range of disk lifetimes.

In the last few years a large number of faint new candidate members of Cha I have been proposed based on their near-infrared (NIR) colors (Cambrésy et al. 1998; Oasa et al. 1999; Persi et al. 2000; Kenyon & Gómez 2001; Gómez & Kenyon 2001; Carpenter et al. 2002). Several of these candidates have been confirmed to be low-mass stars on the basis of their NIR spectra (Gómez & Mardones 2003).

⋆ Tables 2–5 are only available in electronic form at http://www.edpsciences.org

The masses of the presently known Cha I members reach down into the substellar regime, including 13 very-low-mass (VLM) objects at or below the hydrogen burning mass limit discovered in an Hα survey by Comerón et al. (1999). ChaHα 1 (spectral type M 7.5; Comerón et al. 2000, henceforth CNK00) was the first brown dwarf to be detected in X-rays in a *ROSAT* pointed observation (Neuhäuser & Comerón 1998). However, *ROSAT* observations were hampered by low sensitivity and low spatial resolution, and thus unable to constrain the X-ray properties of the VLM Hα sources.

The X-ray emission of VLM stars and brown dwarfs is poorly constrained. In the absence of sensitive observations it is unclear how far the solar-stellar connection reaches into the VLM regime. In particular the influence of mass, temperature, and age on the activity of the coolest stars and the substellar objects remains obscure. The only bona-fide field brown dwarf detected in X-rays so far, LP 944-20, is of intermediate age (500 Myrs), and was revealed with *Chandra* only during a flare (Rutledge et al. 2000). A subsequent deep *XMM-Newton* observation was not able to recover the source (Martín & Bouy 2002) suggesting that this object exhibits only episodic outbursts of activity. The X-ray properties of VLM stars and brown dwarfs on the PMS may be different, because at young ages the atmospheres are hotter, such that more ions are present enhancing the coupling between matter and magnetic field (Mohanty et al. 2002).

Recent deep *XMM-Newton* and *Chandra* observations centered on nearby regions of star formation such as ρ Oph (Imanishi et al. 2001), IC 348 (Preibisch & Zinnecker 2002) and the Orion Nebular Cluster (Feigelson et al. 2002) started to open up the X-ray window to the brown dwarf regime. However, these observations provided at most a few dozen counts per source and/or concern a poorly characterized population of VLM objects. Cha I is one of the nearest star forming regions, with the best-studied group of young brown dwarfs known to date, providing the highest sensitivity yet for the detection of the lowest mass stars and brown dwarfs at young ages.

In this paper we present the *XMM-Newton* observation of the central region of the Cha I South cloud. The observation is described in Sect. 2, where we also outline the steps of the data reduction. The nature of the X-ray sources is discussed in Sect. 3. A detailed spectral analysis is performed for the brighter X-ray sources, and an analysis based on hardness ratios for the fainter X-ray sources (Sect. 4). In Sect. 5 we present our variability study. The results for individual stars and groups of stars are summarized in Sect. 6. Finally, we provide a comparison with earlier *ROSAT* observations of the same field (Sect. 7), and we examine correlations between X-ray emission and stellar parameters (Sect. 8). A summary of our findings is given in Sect. 9.

2. Observations and data analysis

A 30 ks *XMM-Newton* observation centered on the candidate brown dwarf ChaHα 3 was carried out on April 9, 2002 with the European Photon Imaging Camera (EPIC) as prime instrument. EPIC consists of three cameras, two EPIC-MOS detectors and one EPIC-pn detector (see Jansen et al. 2001; Turner et al. 2001; Strüder et al. 2001, for details of the instruments). The observations were performed in full-frame mode employing the thin filter for all components of the EPIC. The Optical Monitor was in blocked position. Data from the Reflection Grating Spectrograph will not be used because we were interested in imaging the star forming region. The field-of-view (FOV) of EPIC comprises all 13 VLM objects in the Cha I region, and also includes a number of higher-mass T Tauri members of the star-forming complex. The observing log for all CCD instruments onboard *XMM-Newton* is given in Table 1.

Table 1. Observing log for the *XMM-Newton* observation of Cha I on April 9, 2002 (Obs-ID 0002740501; Revolution number 427). "Start" and "Stop" refer to start and end of exposures.

Instr.	UT [hh:mm:ss]		JD - 2 452 373		Expo.
	Start	Stop	Start	Stop	[ks]
pn	10:20:23	18:59:59	0.930556	1.290972	31.14
MOS 1	09:47:05	19:03:49	0.907639	1.293750	33.36
MOS 2	09:47:06	19:03:51	0.907639	1.293750	33.36

2.1. Data reduction

As a first step in the data reduction we checked for times of high background. To do so we generated a lightcurve for the whole CCD array, and searched for the limiting acceptable count rate that provides the highest signal-to-noise. We screened data from the three instruments separately, and subsequently applied the resulting good time intervals (GTIs) to the events tables. It turned out that about half of the observing time is contaminated by protons from solar flares. The useful exposure time retained for further analysis is 15.9 ks for pn, and 20.3/20.7 ks for MOS 1/MOS 2 which are less sensitive to high background. The data was filtered for pixel patterns and edge effects at the boundary of individual CCD chips, and a few excessively luminous columns were removed. By eliminating the lowest pulse height channels we further reduced the noise.

After the filtering process we binned images in various energy bands and for all EPIC instruments from the cleaned event files. We used a bin size of 5″ making full use of the spatial resolution of EPIC. We limit our analysis to energies between 0.3−7.8 keV. Below ∼0.3 keV the instrument calibration is not well understood yet. The upper boundary of 7.8 keV avoids the inclusion of additional noise, because for high energies the image is background-dominated. We split the broad band into three energy bands:

soft = 0.3 keV−1.0 keV
hard 1 = 1.0 keV−2.4 keV
hard 2 = 2.4 keV−7.8 keV.

2.2. Source detection

Source detection was performed in all energy bands (soft, hard 1, hard 2, and broad) with the *XMM-Newton* Science Analysis System (SAS) pipeline, version 5.4.1, which employs the box and the maximum likelihood detection algorithm (*eboxdetect* and *emldetect*). First the box algorithm is run in local mode with a low detection threshold. The resulting source list is only used to generate background maps. In the next step all sources above a certain threshold are cut out, the resulting source-free image is rebinned, corrected for spatial exposure variations and smoothed with a two-dimensional spline fit. For this process we eliminated all sources with likelihood >15. Lower threshold values would eliminate a major part of the image such that spline fitting becomes difficult. For the subsequent source detection with *eboxdetect* in map mode we used a *ML* threshold of 8. Then we ran *emldetect* on the source list produced by *eboxdetect* in map mode. For *emldetect* we used a *ML* threshold of 10. However, a known problem in the current version of the *emldetect* code leads to an overestimation of the *ML*. Following the advice in *XMM-Newton* News No. 29, in the final source list we retain only sources with $ML > 20$.

We proceeded in two steps. First all EPIC instruments were analysed separately as described above, then the source detection procedure was applied to the combined files of pn, MOS 1, and MOS 2. Before merging the data of the three detectors we checked the relative alignment of the images by comparing the position of sources common to all three images. We found no systematic displacement. To take account of the different sensitivity of pn and MOS we computed the ratio of count rates measured by pn, MOS 1, and MOS 2 for the brighter sources detected with all three instruments during the first source detection step. In the broad band we found a median ratio pn/MOS ≈ 3.2. The exposure map of pn was then scaled with this value before adding up the files. Differences in the spectral response of MOS and pn were taken into account by determining and applying a separate scaling factor for each energy band: pn/MOS ≈ 4.0 (soft), 2.6 (hard 1), and 2.8 (hard 2). The merged observation corresponds to an equivalent MOS exposure time of ~90 ks in the center of the image.

The merged MOS/pn data contain 58 X-ray sources with $ML > 20$. For further analysis we use the result from the merged data set unless the X-ray source is located outside the FOV, near a chip gap, or in a region of low exposure (such as a bad column) in one or more of the instruments. In these cases we consider the measurement of the individual detector(s) more reliable, and make use of those instruments that do not show any of the above mentioned problems at the respective source position. Table 2 summarizes all 58 detections and their characteristic X-ray parameters. The broad-band counts have been extracted from a circular region of radius 15″ centered on the source. The background counts were obtained from the background map. After the background was subtracted the source counts were corrected for the flux in the PSF wings outside the extraction radius (~30%). The exposure times given in Table 2 were obtained from the broad band exposure map. Hardness ratios are defined and discussed in Sect. 4. The merged EPIC pn and MOS image is shown in Fig. 1, and the position of all detected sources is marked.

3. Nature of the X-ray sources

3.1. Identification of X-ray sources

In the past, membership of the Cha I association has been assigned based on various indicators of youth, such as Hα or X-ray emission, or Li absorption. We searched for counterparts to the *XMM-Newton* X-ray sources in the lists of stellar and substellar Cha I members published by Schwartz (1977), Gauvin & Strom (1992), Hartigan (1993), Huenemoerder et al. (1994), LFH96, and CNK00, which in addition to presenting new members also summarize other previous studies. We also checked for X-ray sources at the position of NIR candidate members suggested by Cambrésy et al. (1998), Comerón et al. (1999), Kenyon & Gómez (2001), Gómez & Kenyon (2001) and Carpenter et al. (2002), the mid-IR ISOCAM sources listed by Persi et al. (2000), and the Cha I candidates from a multi-band optical survey by López Martí et al. (2004). We mention in passing that further faint IR candidates have been published in regions of Cha I outside the FOV of our *XMM-Newton* pointing (e.g. Oasa et al. 1999), which are not of relevance for this study.

For the identification of optical and IR counterparts to the X-ray sources we allowed for a maximum offset of 10″. In total 42 of the X-ray sources have published optical or IR counterparts. Most of the brighter X-ray sources can be clearly identified with known members of the Cha I association. Nearly all spectroscopically confirmed TTS members of Cha I in the FOV, and 9 of 13 VLM Hα objects are detected. Evolutionary models place the dividing line between stars and brown dwarfs at spectral type M 6.5. However, due to uncertainties in spectral classification, spectral type to temperature conversion, and the models themselves, CNK00 have suggested M 7.5 as a conservative location of the substellar boundary in Cha I. Following this approach, the group of VLM Hα objects in Cha I comprises 4 bona fide brown dwarfs, 6 transition objects, and 3 VLM stars. The remaining counterparts to the X-ray sources include some of the recently identified faint NIR candidate members of Cha I. These objects are here shown to be X-ray emitters for the first time. To learn more about the nature of the unidentified sources we searched the 2 MASS archive and found counterparts to an additional five *XMM-Newton* sources. Finally, a search in SIMBAD[1] turned up a BL Lac object as counterpart to XMM-Cha I-35.

A cross-check by visual inspection showed that one probable counterpart was missed by the automatic identification procedure. This source (XMM-Cha I-16) is at the edge of the field, i.e. at large off-axis angle where the point spread function is enlarged. The X-ray source is at a distance of 11.6″ from the cloud member CCE 98-23, detected first in NIR photometry (Cambrésy et al. 1998) and confirmed with a NIR spectrum (Gómez & Mardones 2003). We add this identification to the list in Table 2.

[1] The SIMBAD data base is operated by the CDS and can be accessed via the URL `http://simbad.u-strasbg.fr/sim-fid.pl`

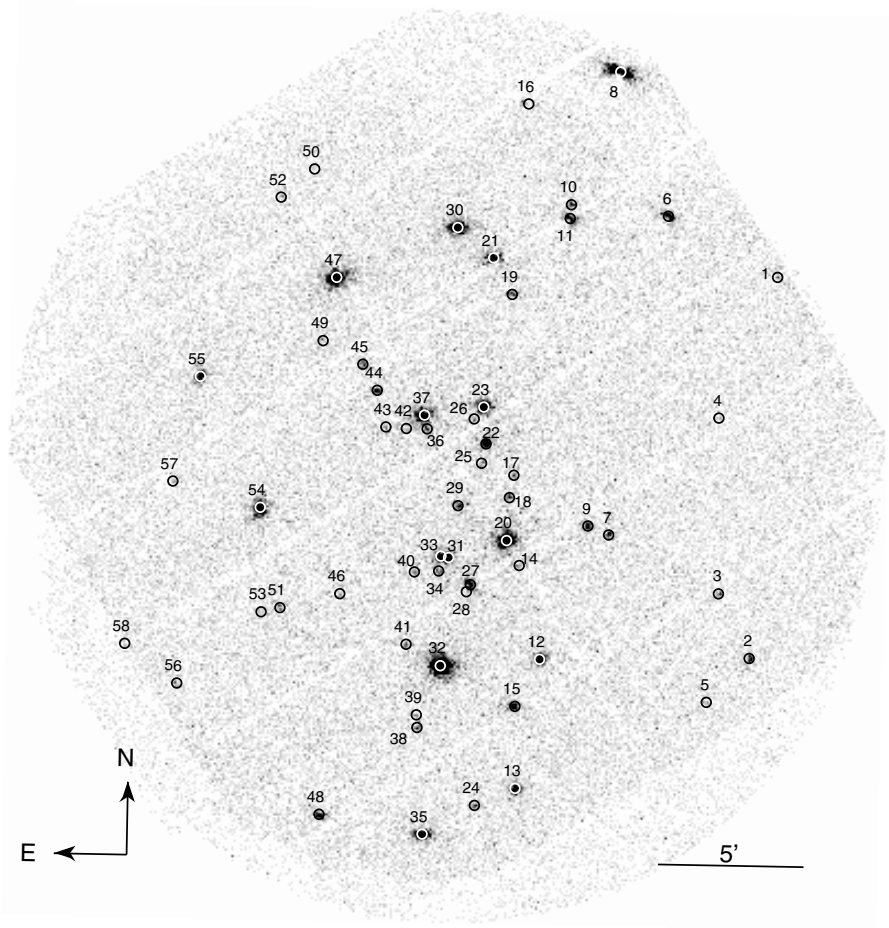

Fig. 1. Merged image of EPIC pn, MOS 1 and MOS 2 for the center of the Cha I South cloud. The positions of all 58 detected sources are marked by circles (radius = 10″). Numbers refer to the designations in Col. 1 of Table 2.

A list with optical/IR data and stellar parameters relevant for the interpretation of the X-ray emission is compiled in Table 3 for all known and potential Cha I members in the *XMM-Newton* FOV. In the following we describe how these parameters were derived.

3.2. Spectral types and extinction

For optically faint stars extinction is often measured in the IR, e.g. through A_J. In the IR dust extinction is composed of both interstellar reddening and absorption by circumstellar material. Determination of the extinction requires knowledge of the spectral type (used to obtain the intrinsic colors from empirical relations), the observed colors, and the assumption of an extinction law. In the ideal case spectral types are directly accessible from optical or IR spectroscopy. We use the spectral types and extinction (A_J, A_I) from the compilation by Gauvin & Strom (1992), and from the spectroscopic surveys by LFH96, Comerón et al. (1999), CNK00, Gómez & Mardones (2003), and Comerón et al. (2004).

For stars for which no spectroscopy is available, the spectral types can be estimated from the photometry in color−color diagrams, projecting the objects back to the locus of unreddened dwarfs. The most widely used transformation between spectral type and intrinsic colors is the one by Bessell & Brett (1988). LFH96 have used this method for a number of X-ray emitting Cha I candidates discovered by *ROSAT*. The X-ray sources seen by *XMM-Newton* comprise some objects for which only visible and IR photometry is available so far: the highly extincted and poorly studied variable star UX Cha, two objects from the NIR survey by Kenyon & Gómez (2001), and five previously unknown objects that we associate with 2 MASS counterparts. In Fig. 2 we show the $J-H/H-K$ color−color diagram for these objects. KG 2001-78 lies bluewards of the reddening band according to the colors given by Kenyon & Gómez (2001). But according to 2 MASS the object seems to be a moderately reddened A-type star. Since KG 2001-78 is rather bright, we suspect that it was saturated in one or more of the bands during the survey by Kenyon & Gómez (2001). Further on we use its 2 MASS photometry.

All 8 objects in Fig. 2 display colors of normal reddened photospheres, without indication for NIR excess from circumstellar material. Note that some of the newly identified 2 MASS counterparts are faint in the NIR ($J \sim 16$ mag; see Table 3), such that the error bars in Fig. 2 extend over the full reddening band, making the assignment of spectral types practically impossible. We deredden the stars in the $J-H/H-K$ diagram along the extinction law of Rieke & Lebofsky (1985)

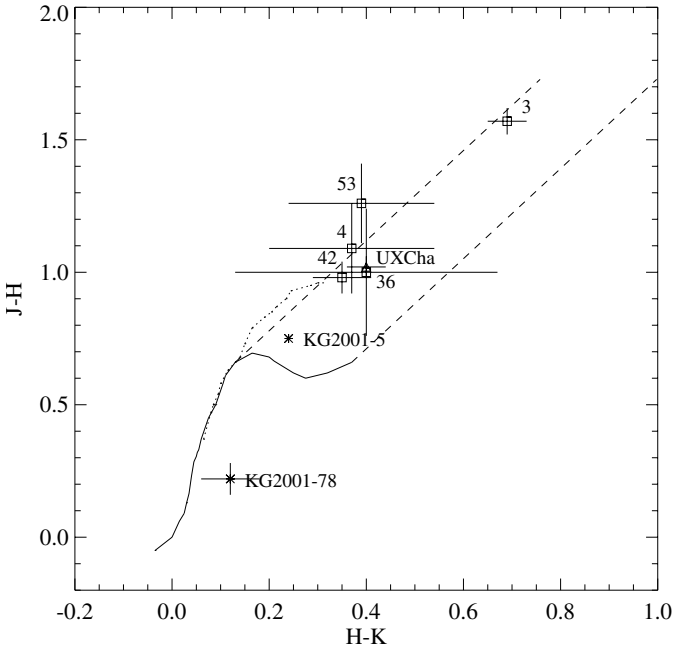

Fig. 2. $J - H/H - K$ diagram showing the position of the eight X-ray detected Cha I candidates without spectroscopic information. The sources with 2 MASS counterparts are labeled with their X-ray source number, objects known before this study are referenced by their previous designation. We use published NIR photometry for KG 2001-5 (Kenyon & Gómez 2001) and 2 MASS data for all other objects. The solid and the dotted curves are the loci of dwarf and giant stars according to Bessell & Brett (1988). The dashed lines indicate a reddening corresponding to $A_V = 10$ mag using the extinction law by RL85.

(hereafter RL85) back to the locus of main-sequence (MS) dwarfs (Bessell & Brett 1988). In the absence of spectroscopy, the ambiguity by the two intersects of the reddening vector with the MS locus cannot be resolved. Based on the faintness of the objects we always assume the later spectral type, but keep in mind that this may lead to an underestimate of A_V by 1−3 mag. Recall also that any possible IR excess is not taken into account, and this would result in an underestimate of the spectral type.

3.3. Physical parameters

In the last columns of Table 3 we list the bolometric luminosity, effective temperature, age, and mass of the stars. Our estimate of the bolometric luminosity is based on the J band magnitude and extinction for stars with spectral type up to M 6, because this band is least affected by IR and UV excess. For objects later than M 6 we use the I band following CNK00's adoption of the Zapatero et al. (1997) empirical color-spectral type relationship. The bolometric luminosity is then given by

$$\log(L_{\rm bol}/L_\odot) = 1.86 - 0.4 \times [J + (V-J)_0 - A_J - DM + BC_V]$$

and an equivalent expression for the I band. The distance modulus is 6.0, corresponding to the distance of 160 pc (Wichmann et al. 1997; Whittet et al. 1997) adopted throughout this paper. The intrinsic colors and bolometric corrections for dwarfs are taken from Kenyon & Hartmann (1995). Beyond spectral type M 6 we use bolometric corrections BC_I as listed by CNK00, which represent a scale intermediate between that of dwarfs and giants. Our luminosity determinations are in good agreement with those published in the literature.

The gravity of PMS stars is intermediate between that of dwarfs and giants. Various temperature scales have been discussed by Luhman & Rieke (1998). We use the spectral type to temperature conversion of Kenyon & Hartmann (1995) for dwarfs. Beyond spectral type M 6 we adopt the intermediate temperatures by Luhman (1999).

Masses and ages are derived in comparison with PMS evolutionary models. Although similar analyses have been performed before by various authors we repeat this exercise in order to have a homogeneous sample that provides consistent *relative* ages and masses for all stars in the *XMM-Newton* field. The only set of PMS tracks that covers the temperature and luminosity range corresponding to the Cha I sample are the models by D'Antona & Mazzitelli (1997). However, these models overestimate the ages of the lowest mass stars. Therefore, we prefer a combination of the calculations by Baraffe et al. (1998) (with initial helium fraction $Y = 0.275$ and initial mixing length parameter $\alpha_{\rm ML} = H_p$) and by Palla & Stahler (1999). Figure 3 shows the *XMM-Newton* sample of Cha I overplotted onto these models. The masses and ages from the Baraffe et al. (1998) tracks and isochrones are adopted for objects with $M < 0.15\ M_\odot$, and those by Palla & Stahler (1999) for all higher-mass stars. A detailed discussion of the masses and ages of the stars in the present sample is outside the scope of this paper. We will use the stellar parameters only to examine correlations with X-ray emission.

The PMS models show that four of the five 2 MASS counterparts to previously unknown X-ray sources are below the zero-age MS assuming a distance of 160 pc, indicating that they may not be related to the Chamaeleon cloud. Their J band magnitudes are in the range of or fainter than those of the VLM members of Cha I suggesting that these sources are located in the background. However, only a spectroscopic study will provide a conclusion on their nature. KG 2001-78 and KG 2001-5, and the 2 MASS counterpart to X-ray source XMM-Cha I-3 are placed for the first time in the HRD. Their position is compatible with their being PMS stars, i.e. they are candidate Cha I members.

4. Spectral analysis

For the spectral analysis source photons were extracted from a circular region centered on the positions given in Table 2, and the background was extracted from an adjacent circular area on the same CCD chip. The source extraction radius was chosen individually such as to achieve high *S/N* without including contamination from neighboring sources. The radii that fullfill these conditions are between 15−30″, with the exception of XMM-Cha I-31 and XMM-Cha I-33 (see Sect. 6.1). Generally, the background extraction region was much larger than the source extraction area, and the background was scaled accordingly. A redistribution matrix and an ancillary response file were calculated for each source using the *XMM*-SAS.

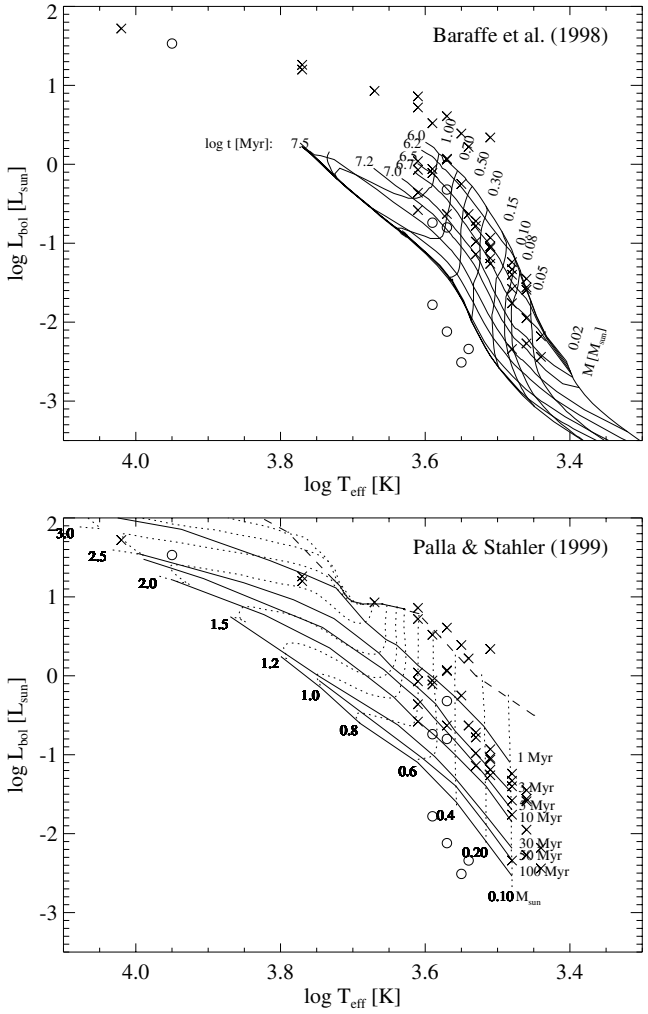

Fig. 3. HRD for counterparts to X-ray sources in the *XMM-Newton* field. Tracks and isochrones that span the full range required to obtain masses and ages for the Cha I sample are from Baraffe et al. (1998) (*top*) and Palla & Stahler (1999) (*bottom*). Counterparts of X-ray sources which have not been spectroscopically studied are shown as circles, and spectroscopic cloud members as *x*-points. The distance assumed is 160 pc.

The spectra were background subtracted and binned to a minimum of 15 counts per bin. For the brighter sources we binned up to 30 counts per bin. Spectral fitting was carried out in the XSPEC environment, version 11.2.0.

We performed a spectral analysis for all X-ray sources with >150 counts in Table 2. This rather low threshold results in considerable uncertainties of the spectral model for the faintest sources of the spectral sample, as a consequence of low statistics. A detailed modelling of the temperature structure in the coronae of our targets is out of reach with the presently available observations. Nevertheless, these *XMM-Newton* data provide for the first time an estimate for the temperature(s) prevailing in the coronae of these stars, and they allow us to identify peculiar X-ray sources.

In most cases we modeled only the EPIC pn spectrum because of its higher sensitivity compared to EPIC MOS. The exception are those sources that are located on chip gaps in the pn. Due to an unfortunate roll-angle this applies to some of the brightest X-ray emitters in this field. For these latter sources we jointly modeled the MOS 1 and MOS 2 spectrum. CHXR-25 falls on a gap in both pn and MOS 2, and we use only MOS 1 for the spectral analysis.

In a first approach we tried to describe each X-ray spectrum with a one-temperature (1-T) thermal plasma model (MEKAL; Mewe et al. 1985; Mewe et al. 1995) plus photoabsorption term with the atomic cross-sections of Morrison & McCammon (1983). Subsolar global abundances from Anders & Grevesse (1989) were chosen motivated by previous results on PMS stars. We adapted the most widely used value of $Z = 0.3\ Z_\odot$ in order to enable direct comparison with previous *Chandra* and *XMM-Newton* studies in other star-forming regions (e.g., Nakajima et al. 2003; Feigelson et al. 2002; Preibisch 2003). Our simplest model has three free parameters: X-ray temperature, emission measure, and hydrogen column density of the absorbing gas.

For some X-ray sources this 1-T model is obviously inadequate (either $\chi^2_{\rm red} > 2$ or there are systematic residuals in a certain spectral range). Allowing the global abundance parameter to vary improves the result in about half of the cases; however, with unreasonably low values for the abundance ($Z \sim 0.05\ Z_\odot$), which we consider unphysical. Adding a second temperature component (2-T model) instead provides a statistically satisfying solution in most cases. Due to the low statistics and the low-energy cutoff of 0.3 keV, for most of the sources the $N_{\rm H}$ values are not well-constrained, and tend to be correlated with the emission measure.

Since our targets are subject to considerable extinction, both from material in the cloud and from circumstellar material, the absorbing column $N_{\rm H}$ is an important parameter. Comparison of the X-ray absorption to measurements of optical extinction can be helpful for checking the X-ray fitting results. All A_J values adopted or computed in this paper are listed in Table 3. We use the RL85 extinction law to obtain $A_{\rm V}$, and the relation by Paresce et al. (1984) to convert $A_{\rm V}$ to hydrogen column density, $N_{\rm H,V}$. Comparing $N_{\rm H,V}$ to the values from the X-ray spectrum ($N_{\rm H,X}$) we find that in about 2/3 of the cases the value expected from the standard galactic relation is bracketed by the 90% error bars provided by the XSPEC fits. Discrepancies arise for some of the X-ray brightest sources, for which $N_{\rm H,X}$ is significantly higher or lower than $N_{\rm H,V}$. However, due to the low-number statistics our data are not sufficient to draw conclusions on a possible deviation from the standard extinction law.

To obtain as homogeneous a set of spectral fits as possible we applied a 2-T model to each source, and held the column density fixed to the value corresponding to the opt./IR value ($N_{\rm H,V}$). These fits also result in acceptable solutions ($\chi^2_{\rm red} \sim 1$), i.e. they cannot be statistically distinguished from the fits with free column density. We consider these latter models more realistic, as motivated below. The best fit parameters for all bright X-ray sources with a counterpart Cha I member or candidate member are summarized in Table 4.

Three objects from the spectral sample have no counterpart among the known or suspected Cha I members, and the thermal model results in a very high X-ray temperature.

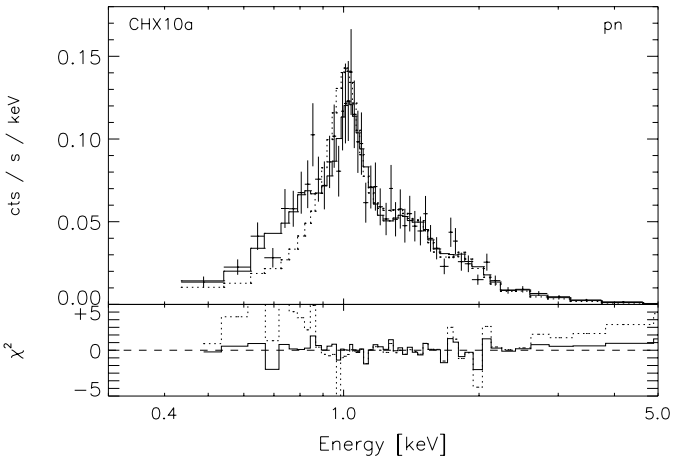

Fig. 4. EPIC pn spectrum of CHX 10a overlaid by the 1-T (dotted histogram) and 2-T (solid histogram) bestfit model. The lower panel shows the χ^2 residuals. Clearly the 1-T model does not adequately describe the data.

One of them (XMM-Cha I-35) is a BL Lac object, the other two have no known optical counterpart in SIMBAD and in the literature. These three objects can be described equally well by a power-law model, consistent with their being extragalactic (see discussion in Sect. 6.6).

4.1. X-ray temperatures and spectral hardness

Among the 25 Cha I sources bright enough for the spectral analysis 12 can be described well by a 1-T model. For 13 stars only adding a second temperature component leads to a fit that is acceptable on the basis of $\chi^2_{\rm red}$ (<2) and upon visual inspection of the residuals. As an example we show in Fig. 4 the pn-spectrum of CHX 10a, one of the stars with the highest *S/N* in this observation, together with the best-fit 1-T and 2-T models. Clearly, the 1-T model is not able to provide a good description of the data in the full energy range.

In all 2-T models the lower temperature tends to be ∼3 MK, and the higher temperature reaches ∼10−15 MK. The temperatures associated with the 1-T models are intermediate between the low and the high energy component of the 2-T models, underlining once more that an iso-thermal plasma is a simplification of the actual coronal temperature structure. This is also obvious from the fact that virtually all X-ray bright objects require the 2-T model. The temperatures are not very sensitive to changes in $N_{\rm H}$, as we can judge from the fact that the kT in the 2-T models with free and with fixed column density do not differ significantly from each other. However, the EM of the soft component depends sensitively on $N_{\rm H}$. We note a few cases where $N_{\rm H,X} > N_{\rm H,V}$, and the high absorption in the fit with free column density is compensated by very high EM of the soft component. Given that these emission measures translate into unrealistically high X-ray luminosities, we consider the fits with $N_{\rm H,V}$ more reliable. All in all, our uniform 2-T models provide a rather stable low-temperature component with ∼3 MK, but the higher temperature shows a larger spread, and there is no universal relation between EM_1 and EM_2, justifying the "definition" of a typical X-ray spectrum for the Cha I stars.

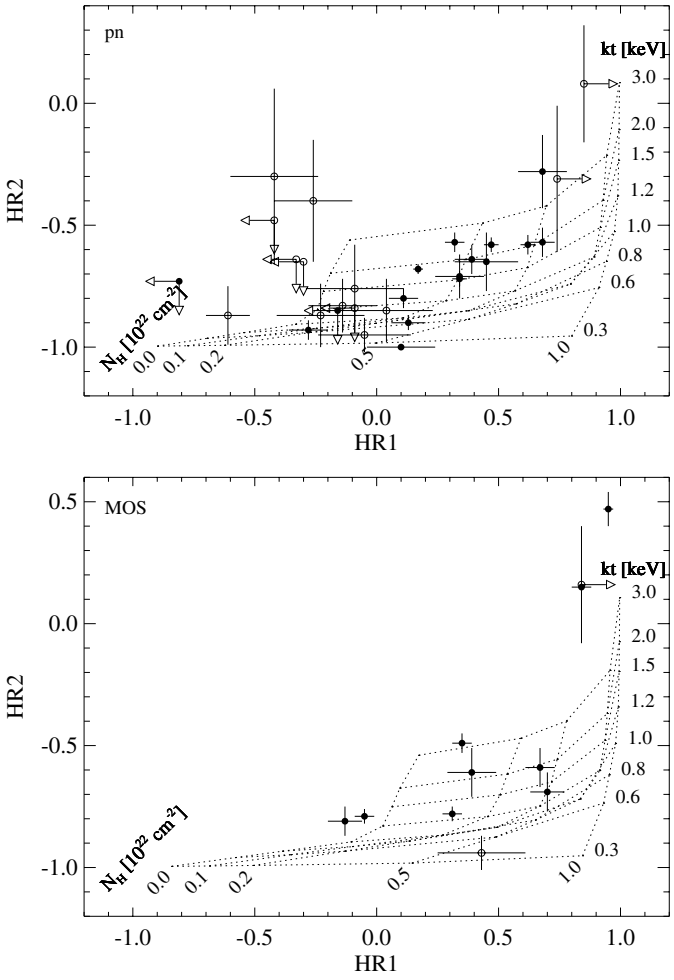

Fig. 5. Hardness ratio diagrams for known Cha I members in the *XMM-Newton* field. *HR* 1 compares the hard 1 (1.0−2.4 keV) and the soft (0.3−1.0 keV) band, and *HR* 2 compares the hard 2 (2.4−7.8 keV) and the hard 1 band. Also shown is a grid of column density and temperature corresponding to the hardness ratios derived from the count rates of a 1-T thermal Raymond-Smith model within PIMMS taking account of the different spectral response of pn (*top panel*) and MOS (*bottom panel*). Hardness ratios for each source are derived from the number of source counts in the respective energy bands: filled circles – bright Cha I members (spectral sample), open circles – faint Cha I members.

30 detections are not bright enough for the analysis of the X-ray spectrum. To obtain an idea about their X-ray temperature we make use of hardness ratios. The hardness ratio is defined as follows: $HR = (A - B)/(A + B)$, where A and B are the numbers of counts in two adjacent energy bands, and A stands for the higher energy. Thus the higher the hardness ratio the harder the spectrum, i.e. the more emission is emitted at high energies. Figure 5 shows the hardness ratios computed for a grid of $N_{\rm H}$ and kT derived from 1-T Raymond-Smith models (Raymond & Smith 1977) using PIMMS[2]. The energy bands are defined as in Sect. 2.1. *HR* 1 compares the hard 1 and the soft band, and *HR* 2 the hard 2 and the hard 1 band. Since the

[2] PIMMS can be accessed via the URL
`http://asc.harvard.edu/toolkit/pimms.jsp`

hardness ratio depends on the spectral response of the detector, pn and MOS data must be regarded separately. For X-ray sources from the merged data set we used the pn hardness ratio because of the higher sensitivity with respect to MOS. Note that the sensitivity to absorption of the hardness ratio derived from any EPIC detector is limited due to the low-energy cutoff at 0.3 keV which is urged by the need to avoid uncertainties in the calibration of EPIC below this threshold.

In Fig. 5 the observed hardness ratios for bright and faint Cha I members (i.e. all detections except the unidentified sources) are shown. As outlined above, most of the bright Cha I stars cannot be successfully fitted by a 1-T model, and their location in the *HR* 1/*HR* 2 diagram is misleading due to the simplifying assumption of an iso-thermal plasma (see discussion in Sect. 4.2). The three X-ray bright objects with the largest *HR* 2 (HD 97048, HM 16, and CCE 98-32) are spatially adjacent to each other, and among the most absorbed stars in this field. The high temperature present in their atmospheres is also apparent in their spectra which are discussed in Sect. 6.1. The faint Cha I stars in Fig. 5 include two candidate members, KG 2001-5 and 2M 110506+773944. Although subject to rather large uncertainties, all but four of the X-ray faint objects (UX Cha, BYB 43, CCE 98-23, and the 2 MASS source) tend to show small $N_{\rm H}$, in agreement with their moderate absorption in the NIR, and display coronal temperatures below ∼2 keV. UX Cha is a poorly studied variable star for which we derive a visual extinction of $A_{\rm V} = 3.2$ mag using 2 MASS photometry in the *JHK* color−color diagram. The 2 MASS counterpart of XMM-Cha I-3 may be a PMS star seen through an extinction of $A_{\rm V} \sim 8$ mag (see Fig. 2). BYB 43 was first detected by IRAS (Baud et al. 1984). Due to its large $K - L$ excess (Kenyon & Gómez 2001) and its very strong Hα emission (Comerón et al. 2004) this object seems to be a cTTS. BYB 43 has a visual extinction of $A_{\rm V} = 7.6$ mag if we transform the A_J given by Comerón et al. (2004) with the RL85 extinction law. Similarly, we find $A_{\rm V} = 30$ mag for CCE 98-23 (Gómez & Mardones 2003). Bearing in mind their high extinction, the (apparently) hard X-ray spectrum of these stars does not come as a surprise.

4.2. X-ray luminosities

We derive individual absorption-corrected X-ray luminosities for each Cha I member and for the X-ray detected candidate members. We chose to compute $L_{\rm x}$ in the 0.4−2.5 keV band to allow comparison with earlier *ROSAT* measurements. The spectra revealed that the Cha I stars emit most of their X-rays below ∼2 keV.

In view of the inhomogeneous statistics of the X-ray spectra it is impossible to determine $L_{\rm x}$ for all stars in the same way. Below we describe the methods used to derive $L_{\rm x}$. The luminosities for the 0.4−2.5 keV band are listed in Table 5, where the method is indicated by the flag in Col. 3. The distance assumed is 160 pc (Whittet et al. 1997). The photon extraction area for the spectral analysis contains between ∼70−85% of the source photons, and accordingly a PSF correction factor was applied to make up for the missing counts.

4.2.1. Bright (spectral) sample

For sources from the bright (spectral) sample $L_{\rm x}$ results directly from the X-ray spectrum. As discussed above, some doubts remain about the best fit due to the existence of several local minima in the χ^2 space. But the fits with column density based on the opt./IR extinction are preferred over the ones with free column density. Table 5 shows the X-ray luminosities $L_{\rm x,V}$ computed from the 2-T best fits with fixed $N_{\rm H,V}$.

Here we want to add some notes to recall the difficulties in establishing reliable X-ray luminosities. When confronting the resulting luminosities $L_{\rm x,V}$ with those where the column density was a free fit parameter ($L_{\rm x,X}$) the following pattern emerges:

- For the sources where the fit with free $N_{\rm H,X}$ requires two temperatures the luminosities $L_{\rm x,X}$ are similar to those from the 2-T fit with fixed $N_{\rm H,V}$, except where $N_{\rm H,X}$ is significantly higher than $N_{\rm H,V}$. In these latter cases $L_{\rm x,X}$ is higher than $L_{\rm x,V}$.
- For sources that can be described with a 1-T model and free $N_{\rm H,X}$ the luminosities are systematically lower than those of the 2-T fit with fixed $N_{\rm H,V}$. We attribute this to the mis-estimate of the temperature and emission measure distribution that is associated with the 1-T model (see discussion in Sect. 4.1).

4.2.2. Faint sample

Since the analysis of the bright sample did not result in a typical spectral shape for a 2-T model, for stars from the faint sample we must rely on assumptions made for the parameters of a 1-T model, and determine the X-ray luminosities from the count rate with the help of PIMMS. We resort to the hardness ratio to guess the spectral model on an individual basis. To check the validity of this approach, we make use of the bright sample, for which we compare the luminosities derived with PIMMS from the 1-T model based on the hardness ratios with the luminosities $L_{\rm x,X}$ extracted from the spectrum. Note that the comparison is based on the spectral fits with free $N_{\rm H,X}$. The reason to use the free-$N_{\rm H,X}$ fits here is that we want to demonstrate the effects of different model assumptions. (Recall, however, that the 2-T fits with fixed $N_{\rm H,V}$ were performed in the most uniform way possible, and are considered more realistic, as explained above.)

The X-ray luminosities derived from the spectral fits on the one hand, and from the hardness ratios on the other hand are shown in Fig. 6. The uncertainties in the X-ray luminosities derive from the uncertainties in $N_{\rm H,X}$. Good agreement between the XSPEC fit results and the PIMMS estimates is found for the luminosities of stars of which the spectra can be described by an iso-thermal model. The discrepancies in Fig. 6 for the stars that require a 2-T model are obvious, underlining that the use of the 1-T grid in the *HR*-diagram is inappropriate. Since virtually all the bright sources, i.e. the ones with good statistics, require two temperatures, we caution that *any* X-ray luminosity derived from an isothermal model may be wrong. The non-linearity of the count-to-energy conversion factor (evident from the curved shape of the model grid in Fig. 5) leads to a systematic underestimation of $N_{\rm H}$ in a 1-T model, and

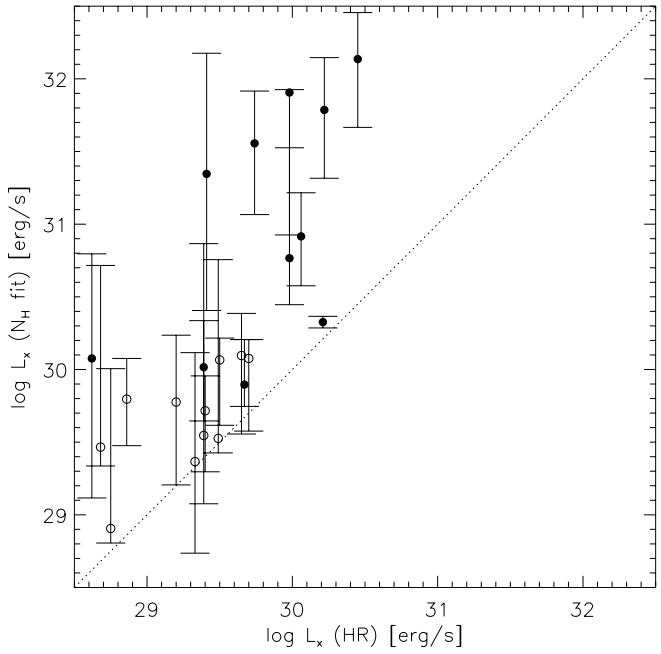

Fig. 6. Comparison of the X-ray luminosities of X-ray bright Cha I objects derived with two different approaches: *x-axis* – using the *HR* to guess the spectral model which is converted to X-ray flux using PIMMS, and *y-axis* – from the X-ray spectrum using XSPEC. Filled plotting symbols denote stars which cannot be described by a 1-T model. As can be seen, for these stars the *HR* tend to provide a wrong estimate of L_x.

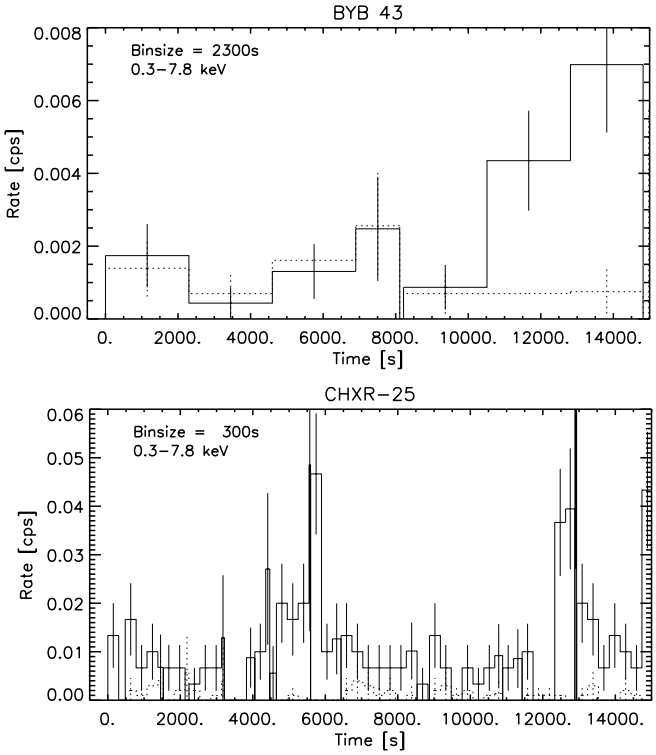

Fig. 7. Broad-band EPIC lightcurve of the cTTS BYB 43 and the wTTS CHXR-25 displaying flares. The dotted line represents the background extracted from an adjacent source-free region. The background has been scaled to the size of the extraction area for the source photons.

consequently the unabsorbed flux is also underestimated. Despite these drawbacks we must nevertheless use this approach for the faint X-ray sources, but be careful with the interpretation of the absolute values for the luminosity.

The location of the objects in the upper left of the range of $N_{\rm H}$ and kT spanned by the grid in Fig. 5 is probably the result of uncertain background level. All these faint sources are M-type stars and brown dwarfs. For these objects we assume a coronal temperature of 0.8 keV (representative for the X-ray spectrum of ChaHα 3, the latest-type object from the bright sample), and a column density corresponding to their individual visual extinction. The luminosity of ChaHα 8, which is not detected in any of the individual detectors but only in the merged pn + MOS image, is computed in the same way, and making use of the response of MOS within PIMMS.

We computed upper limits for the count rates of non-detected Cha I members using the tabulated upper limit counts derived by Gehrels (1986). The upper limit to the flux and luminosity is derived for $kT = 0.8$ keV using the visual/IR absorption if known, else the value estimated from the $J-H/H-K$ diagram (see Sect. 3.2).

5. Time series analysis

For the temporal analysis we used the same photon extraction area as for the spectral analysis. To check for variability we applied the KS-test to the photon arrival times of all X-ray sources in the field after removing data gaps. Variability was examined only within the first 14.5 ks of the observation, because the end of the data set is contaminated by strong background flaring resulting in frequent and long periods without data, interrupted by only short intervals of "good-times". The KS-test was performed in the broad, the soft and the hard 1 band. In the broad band a total of 16 (out of 58) X-ray sources are variable with probability >95%. Most variable sources (14) are Cha I members or candidates. Most of the variability in the broad band can be attributed to the hard 1 band, while the emission in the soft band is more steady. The probabilities for sources which are variable at a significance level >95% are summarized in the last column of Table 5.

Broad, soft, and hard 1 band lightcurves were binned for all variable sources and all other sources with at least >150 counts. Some of the variable stars seem to have undergone irregular variability, others have shown flares. However, there is no evidence for such dramatic outbursts as often reported for low-mass PMS stars (e.g., Skinner et al. 1997; Tsuboi et al. 1998; Stelzer & Huélamo 2000; Hamaguchi et al. 2000). We display two of the most interesting lightcurves in Fig. 7. These examples show that flares occur on cTTS as well as on wTTS. The cTTS BYB 43 is detected for the first time in X-rays, and only because of the flare at the end of the observation. The wTTS CHXR-25 suffered no less than three outbursts during the observing time, amounting to an unusually high flare rate. A number of other interesting variable sources will be discussed in the next section.

6. Individual (groups of) X-ray sources

6.1. The HD 97048 cluster

HD 97048 is a Herbig Ae/Be star with spectral type B9-A0ep+sh (van den Ancker et al. 1998). It is extended in the mid-IR (Prusti et al. 1994) indicating the presence of a dusty envelope. HD 97048 is one of two stars in Cha I with a *HIPPARCOS* parallax. This measurement puts the star at 175^{+27}_{-21} pc (Wichmann et al. 1998).

F93 have identified their X-ray source CHXR-29 with HD 97048. But Zinnecker & Preibisch (1994) argue that the X-ray source is the nearby TTS HM 16 (=Sz 22). In the much longer *ROSAT* pointing presented by Zinnecker & Preibisch (1994) HD 97048 is detected as a weak X-ray source, marginally resolved from HM 16. *XMM-Newton* has clearly resolved these two stars for the first time. In addition, a new X-ray source is discovered close to HM 16. This latter source corresponds to CCE 98-32, an M 2-type star. CCE 98-32 is identical with a visual companion to HM 16 mentioned by Ghez et al. (1997). The separation (16.4″) and position angle (80.2°) we measure between the X-ray sources are in agreement with the values provided by Ghez et al. (1997).

HD 97048 is one of the hardest sources in Fig. 5. A 1-T model does not provide a satisfactory description of the X-ray spectrum ($\chi^2_{\rm red} > 2$). The parameters of the 2-T model indicate strong absorption, a dominating soft component, and a weaker, poorly constrained high-energy tail.

The origin of X-ray emission from HAeBe stars remains mysterious. Several emission meachanism including coronal activity like on late-type stars, strong stellar winds, and unresolved T Tauri companions are being discussed. HD 97048 is not known to be a binary: a Speckle imaging search (Ghez et al. 1997), a spectroscopic search for binarity (Corporon & Lagrange 1999), and spectro-astrometry (Bailey 1998; Takami et al. 2003) have all given negative results. Therefore, the observed X-ray emission is most likely intrinsic to HD 97048. Its origin in a wind is improbable on the basis of its X-ray properties: X-ray emission from stellar wind sources is much softer ($kT \leq 0.5$ keV; Berghöfer et al. 1996) than observed here. HD 97048 was not detected in a VLA survey, unlike several other HAeBe stars for which Skinner et al. (1993) have suggested a thermal wind as the origin of their radio emission.

The two X-ray sources corresponding to HM 16 and CCE 98-32 are too closely spaced for our standard spectral photon extraction procedure. To correct for possible contributions from the respective neighboring source we extracted the background spectrum from an annulus centered on the position of the adjacent contaminating source but exclude the area of the source under consideration. The column density inferred from A_J is $N_{\rm H} > 10^{22}$ cm^{-2} for both stars, consistent with the almost complete lack of photons in the soft band; see also the location of CCE 98-32 and HM 16 at the upper right in the hardness ratio diagram (Fig. 5). As a result the low-temperature component is poorly constrained by the spectral fit, and the numbers for the emission measures and X-ray luminosities of HM 16 and CCE 98-32 in Tables 4 and 5 are uncertain by up to one order of magnitude.

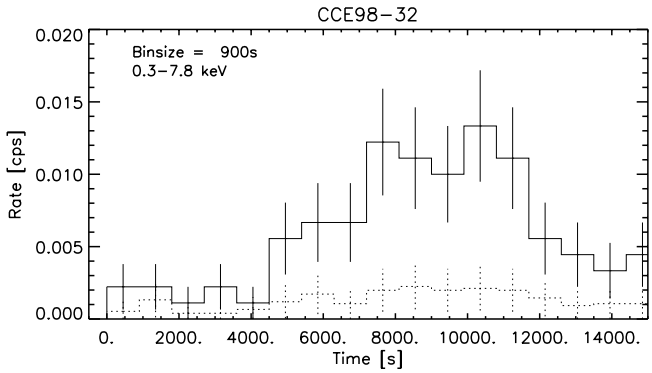

Fig. 8. Broad-band MOS 2 lightcurve of CCE 98-32. The lower curve is the background lightcurve, with count rate scaled corresponding to the extraction area.

According to the KS-test CCE 98-32 is variable in the broad band, but HM 16 and HD 97048 are not. The negative result of the KS-test in the soft and hard 1 band is not surprising, because these stars emit – in contrast to the rest of the Cha I sample – most of their X-rays at energies >1 keV. Inspection of the broad band lightcurve of CCE 98-32 (Fig. 8) shows a smooth and slow increase and subsequent decline of the count rate.

6.2. KG 2001-78

KG 2001-78 is a poorly studied NIR candidate member of Cha I (see Kenyon & Gómez 2001). From its position in the *JHK* color−color diagram we find that this is an A-type star. But, in contrast to HD 97048, no signs of a NIR excess are observed. Among the X-ray sources discussed here it stands out as particularly soft (the hard component is clearly missing) and little absorbed; see Table 4. In Fig. 5 KG 2001-78 is the only object in the bright sample that appears to the left of the unabsorbed 1-T model. We speculate that this might be an indication that its X-ray emission is of different origin. Indeed, its soft spectrum and lack of variability are typical characteristics of wind-driven X-ray sources. The marked difference between the X-ray properties of the only two intermediate mass stars in the FOV (KG 2001-78 and HD 97048) is puzzling, because according to their position in the HRD they have similar mass and age. However, judging from the absence of a NIR excess KG 2001-78 may be more evolved, and activity seems to have ceased, leaving the wind as the only driving mechanism for the X-ray emission.

6.3. Binary T Tauri stars

The *XMM-Newton* FOV comprises some binary systems. LHα332-17, WX Cha, and Glass I are visual binaries according to Ghez et al. (1997) and Chelli et al. (1988). VW Cha is a triple system (Brandeker et al. 2001) with a possible fourth companion (Ghez et al. 1997). The separation in these multiples ranges from the sub-arcsecond regime up to ∼5″, such that all of them are unresolved with *XMM-Newton*.

The TTS Sz 23 is separated from VW Cha by only 16″, and confused with the bright X-ray source at the position of VW Cha in the *XMM-Newton* image.

LFH96 presented two counterparts to the X-ray source CHXR-22. CHXR-22 E is an early M-star, and CHXR-22 W a heavily obscured star with slightly earlier spectral type. Their separation is only 9.5″, so that they are represented by a single X-ray source with *XMM-Newton*. However, the X-ray position is much closer to the Eastern component (see Table 2).

Two of the VLM objects in this field have been listed as possible binaries by Neuhäuser et al. (2002). While the companion candidate ChaHα 5 was later revealed to be a background object (Neuhäuser et al. 2003), Cha Hα 2 might be a binary with a separation of 0.2″.

6.4. Cha IRN

The bipolar reflection nebula Chamaeleon IR nebula is the only spectroscopically confirmed Cha I member in the *XMM-Newton* FOV which is not detected in X-rays. The central object is hidden behind $A_V \sim 10$ mag, and was believed to be an A7....K7 star with an edge-on disk based on IR photometry (Cohen & Schwartz 1984). But a recent NIR spectrum provided a spectral type of M 5 (Gómez & Mardones 2003). The disk may prevent us from seeing the X-ray emission generated by the young star in the center.

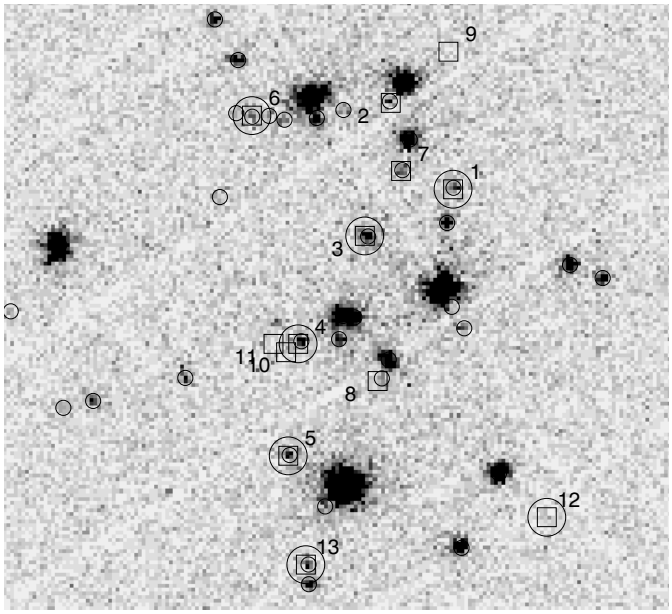

Fig. 9. Merged image of EPIC pn, MOS 1 and MOS 2 showing all VLM Hα emitters in Cha I from the survey by CNK00. The IR positions of Cha Hα 1...13 are indicated by squares and numbers. Small circles are *XMM-Newton* sources, and large circles represent the *ROSAT* PSPC error boxes of 25″ radius at the IR position of those ChaHα objects detected with *ROSAT*; no *ROSAT* X-ray positions are given in the literature.

6.5. VLM Hα stars and brown dwarfs

CNK00 list 7 of the 13 VLM Hα emitters in Cha I as X-ray detections. As mentioned in Sect. 3 we detected 9 of these objects with *XMM-Newton*. With the exception of ChaHα 12, which is not detected with *XMM-Newton*, all *ROSAT* sources are confirmed. *XMM-Newton* revealed for the first time X-ray emission from ChaHα 2, ChaHα 7 and ChaHα 8. These three objects may have escaped detection with *ROSAT* because they could not be resolved from nearby bright TTS. ChaHα 4 appeared as an elongated object in the *ROSAT* image. With the improved spatial resolution of *XMM-Newton* we can separate it from ChaHα 10 and ChaHα 11. We find that these last two are not detected, and the only X-ray source can be clearly attributed to ChaHα 4. A visual comparison of the *ROSAT* and *XMM-Newton* detections is given in Fig. 9.

Only one of the objects at the substellar borderline, ChaHα 3, which was the prime target of this pointing, has enough statistics to attempt modeling the X-ray spectrum. Analogous to (many of) the higher-mass Cha I members with similar numbers of counts ChaHα 3 can be described with a single-temperature MEKAL model and a photo-absorption term. The X-ray temperature (∼9 MK) is indistinguishable from those of the higher-mass TTS. But a 2-T model with column density fixed at the values calculated from the opt./IR extinction fits the data equally well, and provides typical parameters for late-type stars (see Tables 4 and 5). For the remaining detected ChaHα objects the hardness ratios indicate comparatively soft X-ray spectra, i.e. moderate X-ray temperature and low absorption. But this may be a selection effect: all VLM objects in Cha I discovered so far are located in regions of low extinction.

The VLM stars and brown dwarfs in Cha I do not appear either to differ from the higher mass stars in terms of their variability: according to the KS-Test 2 out of 9 detected objects with spectral type later than M 4 are variable, while 12 out of 29 higher-mass stars are variable. Therefore, the variability of the VLM objects seems to be similar to that of the higher-mass TTS. This is in contrast to the observation of old brown dwarfs in the field: the only field brown dwarf detected so far in X-rays was observed during a flare, but later observations found only a very restrictive upper limit to its X-ray luminosity (Rutledge et al. 2000; Martín & Bouy 2002).

However, we point out that the two strongly variable VLM stars ChaHα 13 (spectral type M 5) and ChaHα 8 (spectral type M 6.5) have undergone flares (Fig. 10). For ChaHα 13 the lightcurve shows that most of the source photons are concentrated in two distinct events near the middle of the observation. The duration of these events ∼1/2 h is typical for X-ray flares on late-type stars (Stelzer et al. 2000). ChaHα 8 has flared at the beginning of the observation. Outside these events both sources emerge barely from the background level. In contrast the X-ray brightest of the VLM objects, ChaHα 3, is clearly detected throughout the observing time.

6.6. Unidentified X-ray sources

For four X-ray sources not associated with any Cha I star or candidate from the literature we found a 2 MASS counterpart that does not seem to be a cloud member according to

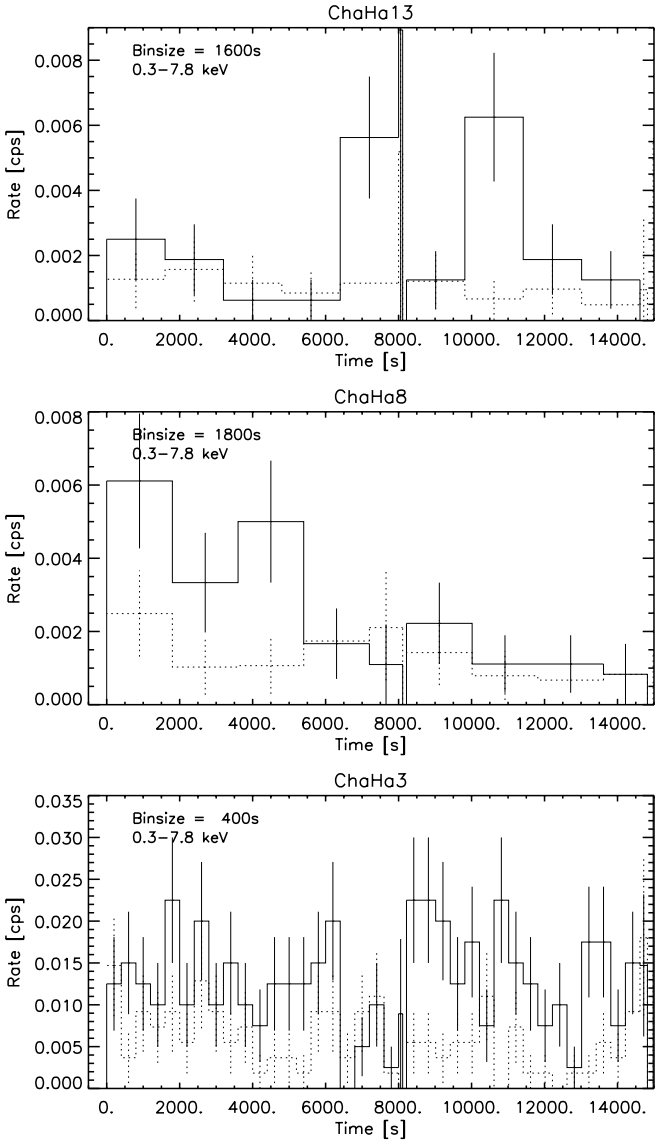

Fig. 10. Broad-band X-ray lightcurves of three VLM objects in Cha I: ChaHα 13 and ChaHα 8 barely emerge from the background outside flares, while ChaHα 3 is clearly visible throughout the observing time.

its position in the HRD (see Fig. 3 and Table 3). These objects lie slightly below the zero-age MS, and are underluminous by ∼1 order of magnitude with respect to Cha I members of similar effective temperature. It may be worth mentioning that Comerón et al. (2003) identified young stars in the Lupus star forming region with bolometric luminosity lower than expected for their age or, in other words, stars that according to their position in the HR diagram appear older than expected. Hartmann et al. (1997) showed that strong accretion may accelerate stellar evolution, and, indeed, the underluminous objects in Lupus display unusually strong Hα emission. If we take X-ray emission as a proxy for youth, the same mechanism may be at work in the 2 MASS objects in Cha I. However, we lack information on their accretion properties. Moreover, the NIR photometry used to place them in the HR diagram introduced large uncertainties in both spectral type, i.e. effective temperature, and luminosity

Table 6. Best fit parameters of an absorbed power-law model for X-ray bright unidentified X-ray sources in the Cha I *XMM-Newton* field.

Designation	$\chi^2_{\rm red}$ (d.o.f.)	$N_{\rm H}$ [10^{22} cm^{-2}]	Γ	$f_{\rm x}$ [erg/cm^2/s]
XMM-Cha I-18	0.91 (3)	3.4	2.76	1.6×10^{-13}
XMM-Cha I-35	0.89 (25)	0.91	1.47	3.4×10^{-13}
XMM-Cha I-44	0.80 (6)	0.73	1.73	4.0×10^{-14}

(via extinction). Conclusions about their nature that go beyond our speculative remarks require a spectroscopic investigation.

Only one X-ray source could be identified with a known extragalactic object, the BL Lac source WGA J1108.1-774 (Perlman et al. 1998). Another 11 X-ray sources remain without optical/IR counterpart.

Within this sample of X-ray sources not confirmed to be Cha I members three are bright enough for the analysis of the spectrum: the BL Lac object, and two of the unidentified X-ray sources. For all of them a thermal model results in unusually high and poorly constrained X-ray temperature, although the statistics of the spectrum are comparable to that for some of the known Cha I stars in the field. We fitted these spectra alternatively with an absorbed power law. The power law indices are between 1.5...2.7 (see Table 6), which is typical for extragalactic sources (Tozzi et al. 2001).

For the remaining unknown X-ray objects we examined the hardness ratios (Fig. 11). Most of the objects cluster in a region in the upper right of the area spanned by the thermal model. The fact that they are harder than typical coronal emitters (compare Fig. 5) may indicate that these are extragalactic sources. The typical flux level of the unidentified objects is $\sim 10^{-14}$ erg/s/cm^2. According to the $\log N - \log S$ distribution presented by Hasinger et al. (2001) a total of ∼20 extragalactic sources is expected at this flux-level within the *XMM-Newton* field, in rough agreement with the number of unidentified X-ray sources.

On the other hand, two among the most highly extincted Cha I stars (HM 16 and CCE 98-32) showed similar hardness ratios and an X-ray spectrum with a very pronounced high-energy tail (see Fig. 5 and Sect. 6.1). Therefore we caution that several cloud members may still be hidden behind substantial extinction. Gómez & Mardones (2003) argued on the basis of the apparent fall-off of the mass function in Cha I that up to ∼100 low-mass stars and brown dwarfs remain to be identified in this cloud. Some of these stars may be among the IR candidate members presented in the literature, and among the unidentified *XMM-Newton* sources.

7. Comparison to *ROSAT*

In searching for long-term variability we compare the *XMM-Newton* observation of April 2002 to earlier X-ray observations of the same stars. The full EPIC FOV was covered 11 yr earlier in two pointings with the *ROSAT* PSPC. The results of the *ROSAT* observations were discussed by F93, Neuhäuser et al. (1999), and CNK00. In the absence of statistics that would

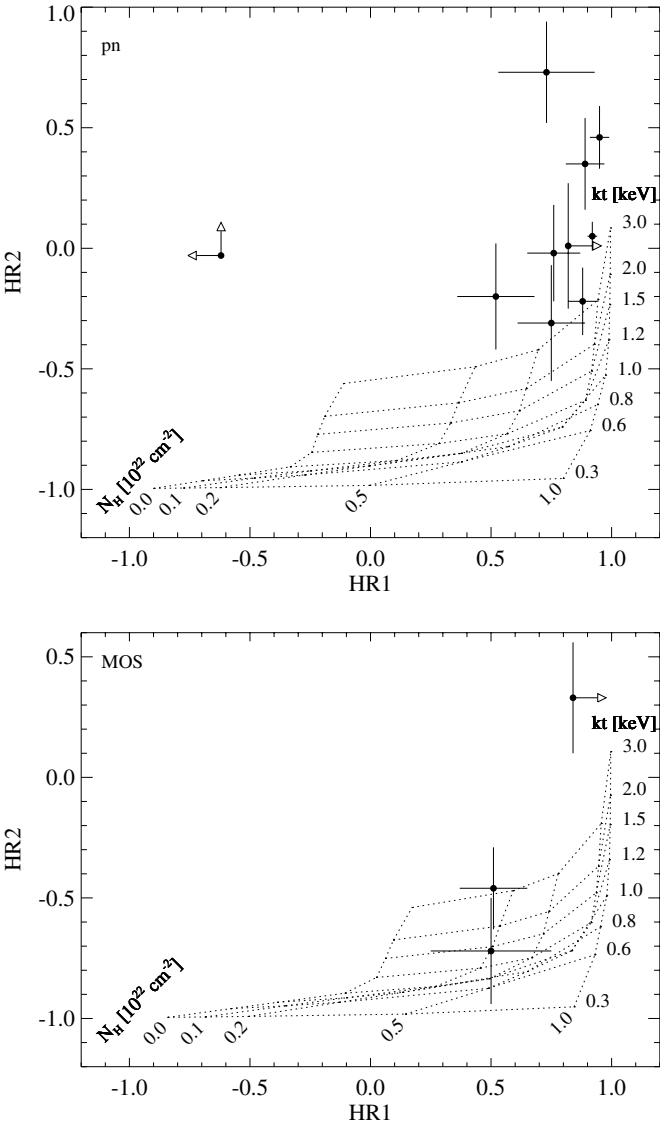

Fig. 11. EPIC pn and MOS hardness ratios for unidentified X-ray sources overplotted on a grid of column density and temperature for a 1-T thermal model; see Fig. 5 and text in Sect. 4.1 for more details. Most objects are harder than typical spectra for the bulk of Cha I stars, suggesting either very young and strongly absorbed cloud members or extragalactic origin (see text in Sect. 6.6).

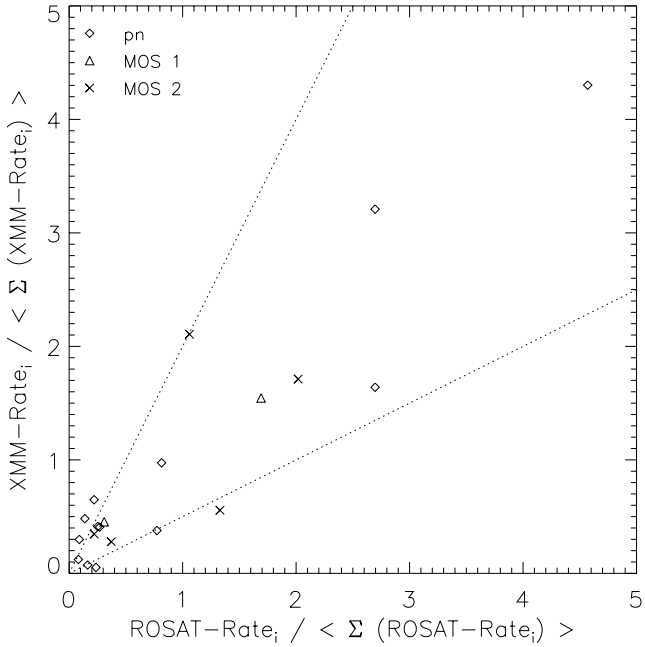

Fig. 12. Relative X-ray brightness of stars in Cha I during the *XMM-Newton* and the *ROSAT* observation. Count rates refer to the 0.4–2.5 keV band. Only stars detected by both satellites are shown. The dotted lines embrace variations by a factor two and less.

allow a spectral analysis F93 derived the X-ray luminosities assuming a 1 keV plasma seen through an absorbing column of 0.2×10^{22} cm^{-2} for *all* X-ray sources. LFH96 presented new optical photometry and spectroscopy, updated the list of Cha I members, and compiled L_x for this new list following the assumptions on the spectral shape by F93.

The luminosities measured by F93 and LFH96 with *ROSAT* are systematically lower than those we derive from the *XMM-Newton* spectra, in some cases by more than one order of magnitude. This is probably the effect of a serious underestimation of the absorption in the low-sensitivity *ROSAT* observations. In view of the difficulties in establishing luminosities based on simplified models we prefer to compare the data at the count rate level. We normalized the count rate of each X-ray source by the mean count rate of the total sample, separately for *XMM-Newton* and *ROSAT*. This quantity characterizes the brightness of the source with respect to the whole sample, and should remain approximately constant over time. In Fig. 12 we confront the values derived from the two satellites with each other. The data scatter around the 1:1 relation with little indications for variations larger than a factor of two, signaling that there is no significant long-term variability.

8. Correlation with stellar parameters

The ratio of X-ray to bolometric luminosity is one of the most widely used activity indicators. Previous studies have repeatedly found that $L_x/L_{bol} \sim 10^{-3}$ for the most active stars, with a scatter of ~2 dex down to $L_x/L_{bol} \sim 10^{-5}$ for less active stars. This "saturation" is well-established on the basis of *ROSAT* observations in various star forming regions. In Cha I a linear regression to $\log L_x$ versus $\log L_{bol}$ gave a slope of 1.4×10^{-4} (see F93). However, as a consequence of the underestimation of the X-ray luminosities of Cha I stars in *ROSAT* measurements, this mean L_x/L_{bol} value as well as the saturation level must now be questioned.

We examine the L_x/L_{bol} relation combining the *XMM-Newton* data with the L_{bol} values derived in Sect. 3.3. The result is shown in Fig. 13. The well-known correlation between L_x and L_{bol} is evident, with the common scatter of ~2 dex. The net effect of our more realistic X-ray luminosities is shifting the correlation by ~1 dex upwards, such that nearly all stars end up with $L_x/L_{bol} > 10^{-4}$. Stars for which L_x has been determined from the spectrum (symbolized by filled circles in Fig. 13) tend to have high L_x/L_{bol}, with saturation near $10^{-2.5}$. For stars with too little signal for an analysis of the X-ray spectrum (open plotting symbols in Fig. 13)

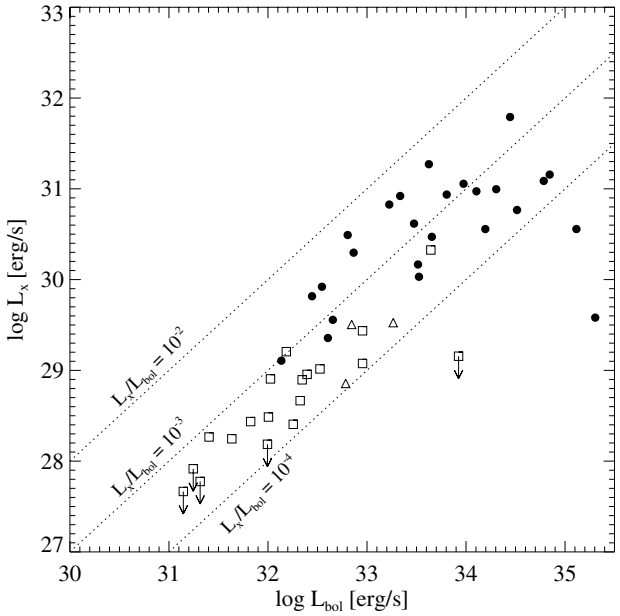

Fig. 13. X-ray versus bolometric luminosity. Different plotting symbols denote different methods to derive L_x: filled circles – spectral fits with 2-T models and column density derived from A_J; open squares – assumed 1-T model with $\log T = 6.95$ and A_J from the literature; open triangles – assumed 1-T model with $\log T = 6.95$ and A_J derived from the *JHK* color−color diagram (Fig. 2).

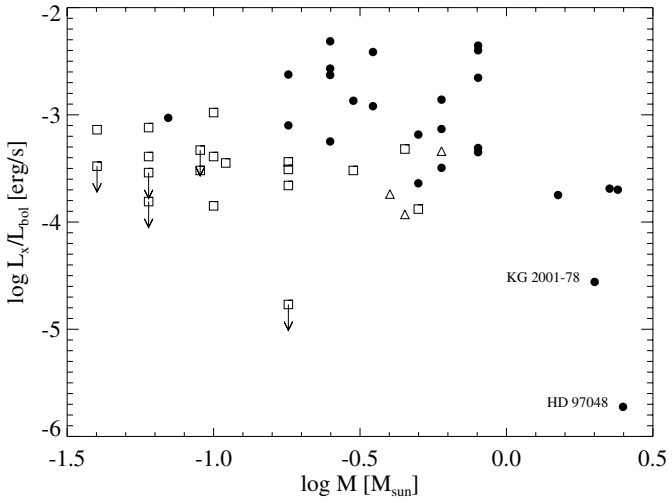

Fig. 14. Ratio of X-ray to bolometric luminosity versus mass derived from the PMS models by Baraffe et al. (1998) and Palla & Stahler (1999). The meaning of the plotting symbols is the same as in Fig. 13. Note the large spread for intermediate-mass which likely reflects directly the changes in the interior structure.

L_x was derived *assuming* a spectral model, and the saturation level is found to be $\sim 10^{-3}$. The most obvious explanation is a bias introduced by the simplified model assumptions: in particular the assumption of an isothermal plasma and uniform extinction lead to an underestimate of the emission measure. As a consequence the true saturation level of the faint stars in Cha I could be similar to that of the brighter Cha I members. However, a physical effect, i.e. changing saturation level with stellar mass, cannot be excluded from the data. Indeed, this latter interpretation would be in accordance with a *Chandra* study of the Orion Nebula Cluster which suggested that L_x/L_{bol} declines at the low-mass end of the MS (Flaccomio et al. 2003b).

The two outliers in Fig. 13 with the highest bolometric luminosity are the intermediate mass stars HD 97048 and KG 2001-78, which may be subject to different X-ray emission mechanisms. A similar trend was seen in a *Chandra* observation of the young NGC 1333 cluster. Preibisch & Zinnecker (2002) argued that a bifurcation seen for stars with high bolometric luminosity in the $L_x - L_{bol}$ diagram is produced by A-type stars with late-type companions. In our case the companion hypothesis is improbable: HD 97048 is a well-studied single star, and KG 2001-78 shows an X-ray spectrum very distinct from that of a TTS. A large spread of $\log(L_x/L_{bol})$ was also reported for intermediate mass stars in Orion (Feigelson et al. 2003; Flaccomio et al. 2003b), giving rise to the speculation that, depending sensitively on the details of the internal structure, various emission mechanisms may be at work in this critical mass range. This view seems to be supported by our observation of just two, but apparently very different, A-type X-ray emitters in Cha I.

We also examined the relation between X-ray luminosity and stellar age. Most of the stars are found in a small age range between ∼2−6 Myr. The near-to coevality of the Cha I population and its implication on the star formation rate has been discussed by LFH96. The need for a strong increase of the star formation rate in the past can be avoided if the older population is incomplete, e.g. because the stars have dispersed and thus escaped recognition as a cloud member. Interestingly, three of the four undetected VLM ChaHα objects have ages >10 Myr. From the presently derived upper limits we cannot say whether the dynamo of the lowest mass stars and brown dwarfs has completely shut off at this age, or if these objects just follow a trend of declining X-ray luminosity with age.

It has been argued that the decrease of L_x with age may be an effect of the loss of coupling between the increasingly neutral atmosphere and the magnetic field (Mohanty et al. 2002). We find no evidence for a temperature related dynamo shut-off for the lowest masses: the undetected VLM objects have effective temperatures comparable to the detected VLM objects. For the whole sample a strong correlation between L_x and T_{eff} is evident. However, this correlation disappears if L_x is replaced by L_x/L_{bol}. Therefore, the $L_x - T_{eff}$-correlation can be explained by the dependence of L_{bol} on T_{eff} together with the relatively small scatter of the stars in terms of L_x/L_{bol}.

Finally, the relation of X-ray emission with stellar mass is shown in Fig. 14. This diagram shows that the spread in L_x/L_{bol} increases dramatically for intermediate-mass stars: the less evolved ones still possess substantial convection zones, and display X-ray emission levels similar to lower-mass stars. KG 2001-78 and HD 97048 are in their final approach to the MS, fully radiative, and consequently less active. A similar trend was found in the ONC by Flaccomio et al. (2003b) and Feigelson et al. (2002).

9. Summary

In a 30 ks *XMM-Newton* observation of the Cha I South cloud we detected the intermediate-mass HAeBe star HD 97048, all known TTS members except Sz 23 (confused with VW Cha) and the IR Nebula, most of the VLM Hα objects near or below the substellar limit, and three photometric Cha I candidates, two of which are probably late-type stars and one is likely to be an A-type star. A possibly sub-Jupiter mass object recently proposed as a Cha I candidate by Comerón & Claes (2004) is in the central part of the *XMM-Newton* field, but not detected.

Our X-ray detection of candidate young stars identified by means of NIR photometry is an important indication for them being true members of the star forming region. We argue on the basis of their X-ray properties that some additional new cloud members may be among the unidentified X-ray sources. The nature of these objects as well as of the detected NIR candidate members will be revealed in optical/IR follow-up studies.

We performed a detailed spectral analysis of the brighter half of the Cha I members in the *XMM-Newton* field. The spectra are described by thermal emission from a hot, optically thin plasma, and a photo-absorption term taking account of interstellar and/or circumstellar extinction. Absorbing column densities derived from *Chandra* and *XMM-Newton* spectra were used by Vuong et al. (2003) to constrain the gas-to-dust extinction relation. Their analysis of X-ray data from various star forming regions showed that in ρ Oph the measured $N_{\rm H,X}$ are systematically lower than expected from A_J assuming the standard value of $N_{\rm H}/A_{\rm V} = (1.8{-}2.2) \times 10^{21}$ cm^{-2} per magnitude; see references in Vuong et al. (2003). Their sample in Cha I comprised only 4 reasonably X-ray bright stars in the northern cloud observed with *Chandra*, that span a small range in optical extinction. We point out that low absorption is not a general characteristic of the Cha I cloud. In fact, the *XMM-Newton* FOV contains some objects with $A_{\rm V} > 10$ mag. But the statistics in their X-ray spectra are too small to derive a well-constrained $N_{\rm H}$. We consider the spectral fits with column density fixed on the value expected from the canonical $N_{\rm H} - A_{\rm V}$ relation more reliable, and feel that the interpretation of the $N_{\rm H} - A_{\rm V}$ relation based on present-day X-ray observations demands caution.

The X-ray temperatures of the coronal sources in Cha I are similar to those found by Favata et al. (2003) in the Taurus cloud L 1551, but lower than those found in recent X-ray observations of IC 348 (Preibisch & Zinnecker 2002), NGC 1333 (Getman et al. 2002), and the Orion Nebula Cloud (Feigelson et al. 2002). This can probably be attributed to the use of different instruments and model assumptions. The latter three studies are based on *Chandra* and adopted a 1-T approach. It is a well-known fact that 1-T models do not represent a valid description of the temperature structure in stellar coronae. Nevertheless, they are often used to describe low-resolution X-ray spectra with low numbers of counts. We find that 1-T models have a tendency to underestimate $L_{\rm x}$ because they underestimate absorption. For this reason we chose to describe all Cha I members which are bright enough for spectral analysis by a 2-T model. Not surprisingly our spectral analysis yielded systematically higher X-ray luminosities as compared to the previous estimates derived from *ROSAT* observations. The X-ray luminosities of the low-mass stars in Cha I have now been re-adjusted, and reveal a saturation level near $10^{-2.5...-3}$ (versus $\sim 10^{-4}$ suggested by *ROSAT*). On the basis of this conclusion is it impractical to engage in a study of long-term variability based on X-ray luminosities. We have, however, no signs for variability exceeding a factor of $\sim$2 within the last 11 yr.

The confirmation of X-ray emission from all but one of the *ROSAT* detected VLM ChaHα objects provides important support for the reliability of the *ROSAT* source detection process. ChaHα 7 is the first M 8 brown dwarf in Cha I detected in X-rays. In addition, the higher sensitivity and continuous data stream of *XMM-Newton* has allowed us for the first time to examine the spectral characteristics and the time variability of the latest type stars and brown dwarfs in Cha I. We find no evidence for a dramatic change in the X-ray properties (such as X-ray temperature and X-ray luminosity) at the substellar limit. The oldest VLM objects are undetected, presumably due to the decline of X-ray luminosity with age, and not to an effect of the atmospheric temperature. In terms of variability the lowest mass Cha I members behave similar to higher-mass TTS in the cloud. In particular they are shown to undergo flares.

Acknowledgements. B.S. acknowledges financial support from the European Union by the Marie Curie Fellowship Contract No. HPMD-CT-2000-00013. B.S. wants to thank F. Comerón and J. Alves for discussions on the IR properties of young stars, and K. Briggs and I. Pillitteri for discussions on the data analysis. We thank the referee, F. Comerón, for very careful reading and useful comments on essential points. *XMM-Newton* is an ESA science mission with instruments and contributions directly funded by ESA Member States and the USA (NASA).

References

Anders, E., & Grevesse, N. 1989, Geochim. Cosmochim. Acta, 53, 197
Bailey, J. 1998, MNRAS, 301, 161
Baldi, A., Molendi, S., Comastri, A., et al. 2002, ApJ, 564, 190
Baraffe, I., Chabrier, G., Allard, F., & Hauschildt, P. H. 1998, A&A, 337, 403
Baud, B., Beintema, D. A., Wesselius, P. R., et al. 1984, ApJ, 278, L53
Berghöfer, T. W., Schmitt, J. H. M. M., & Cassinelli, J. P. 1996, A&A, 118, 481
Bessell, M. S., & Brett, J. M. 1988, PASP, 100, 1134
Brandeker, A., Liseau, R. Artymowicz, P., & Jayawardhana, R. 2001, ApJ, 561, L199
Cambrésy, L., Copet, E., Epchtein, N., et al. 1998, A&A, 338, 977
Carpenter, J. M., Hillenbrand, L. A., Skrutskie, M. F., & Meyer, M. R. 2002, AJ, 124, 1001
Chelli, A., Zinnecker, H., Cruz-Gonzalez, I., Carrasco, L., & Perrier, C. 1988, A&A, 207, 46
Cohen, M., & Schwartz, R. D. 1984, AJ, 89, 277
Comerón, F., & Claes, P. 2004, ApJ, 602, 298
Comerón, F., Rieke, G. H., & Neuhäuser, R. 1999, A&A, 343, 477
Comerón, F., Neuhäuser, R., & Kaas, A. A. 2000, A&A, 359, 269 (CNK00)

Comerón, F., Fernández, M., Baraffe, I., Neuhäuser, R., & Kaas, A. A. 2003, A&A, 406, 1001
Comerón, F., Reipurth, B., Henry, A., & Fernández, M. 2004, A&A, 417, 583
Corporon, P., & Lagrange, A.-M. 1999, A&AS, 136, 429
D'Antona, F., & Mazzitelli, I. 1997, MemSAI, 68, 807
den Herder, J. W., Brinkman, A. C., Kahn, S. M., et al. 2001, A&A, 365, L7
Favata, F., Giardino, G., Micela, G., Sciortino, S., & Damiani, F. 2003, A&A, 403, 187
Feigelson, E. D., & Kriss, G. A. 1989, ApJ, 338, 262
Feigelson, E. D., Casanova, S., Montmerle, T., & Guibert, J. 1993, ApJ, 416, 623 (F93)
Feigelson, E. D., Broos, P., Gaffney, J. A., et al. 2002, ApJ, 574, 258
Feigelson, E. D., Gaffney, J. A., Garmire, G., et al. 2003, ApJ, 584, 911
Flaccomio, E., Micela, G., & Sciortino, S. 2003a, A&A, 397, 611
Flaccomio, E., Damiani, F., Micela, G., et al. 2003b, ApJ, 582, 398
Gauvin, L. S., & Strom, K. M. 1992, ApJ, 385, 217
Gehrels, N. 1986, ApJ, 303, 336
Getman, K. V., Feigelson, E. D., Townsley, L., et al. 2002, ApJ, 575, 354
Ghez, A. M., McCarthy, D. W., Patience, J. L., & Beck, T. L. 1997, ApJ, 481, 378
Gómez, M., & Mardones, D. 2003, AJ, 125, 2134
Gómez, M., & Kenyon, S. 2001, AJ, 121, 974
Hamaguchi, K., Terada, H., Bamba, A., & Koyama, K. 2000, ApJ, 532, 1111
Hartigan, P. 1993, AJ, 105, 1511
Hartmann, L., Cassen, P., & Kenyon, S. J. 1997, ApJ, 475, 770
Hasinger, G., Altieri, B., Arnaud, M., et al. 2001, A&A, 364, L45
Henize, K. G., & Mendoza, E. E. 1973, ApJ, 180, 180
Huenemoerder, D., Lawson, W. A., & Feigelson, E. D. 1994, MNRAS, 271, 967
Imanishi, K., Tsujimoto, M., & Koyama, K. 2001, ApJ, 563, 361
Jansen, F., Lumb, D., Altieri, B., et al. 2001, A&A, 365, L1
Kenyon, S., & Gómez, M. 2001, AJ, 121, 2673
Kenyon, S., & Hartmann, L. 1995, ApJS, 101, 117
Kraft, R. P., Burrows, D. N., & Nousek, J. A. 1991, ApJ, 374, 344
Lawson, W. A., Feigelson, E. D., & Huenemoerder, D. P. 1996, MNRAS, 280, 1071 (LFH96)
López Martí, B., Eislöffel, J., Scholz, A., & Mundt, R. 2004, A&A, 416, 555
Luhman, K. L. 1999, ApJ, 525, 466
Luhman, K. L., & Rieke, G. H. 1998, ApJ, 497, 354
Martín, E. L., & Bouy, H. 2002, New Astron., 7, 595
Martín, E. L. 1998, AJ, 115, 351
Mewe, R., Gronenschild, E. H. B. M., & van den Oord, G. H. J. 1985, A&AS, 62, 197
Mewe, R., Kaastra, J., S., Schrijver, C. J., van den Oord, G. H. J., & Alkemade, F. J. M. 1995, A&A, 296, 477
Mohanty, S., Basri, G., Shu, F., Allard, F., & Chabrier, G. 2002, ApJ, 571, 469
Morrison, R., & McCammon, D. 1983, ApJ, 270, 119
Nakajima, H., Imanishi, K., Takagi, S.-I., Koyama, K., & Tsujimoto, M. 2002, PASJ, 55, 635
Neuhäuser, R., Brandner, W., Alves, J., Joergens, V., & Comerón, F. 2002, A&A, 384, 999
Neuhäuser, R., Guenther, E. W., & Brandner, W. 2003, in Brown Dwarfs, ed. E. L. Martín, IAU Symp., 211, 309
Neuhäuser, R., Briceño, C., Comerón, F., et al. 1999, A&A, 343, 883
Neuhäuser, R., & Comerón, F. 1998, Science, 282, 83
Oasa, Y., Tamura, M., & Sugitani, K. 1999, ApJ, 526, 336
Palla, F., & Stahler, S. W. 1999, ApJ, 525, 772
Paresce, F. 1984, AJ, 89, 1022
Perlman, E. S., Padovani, P., Giommi, P., et al. 1998, AJ, 115, 1253
Persi, P., Marenzi, A. R., Olofsson, G., et al. 2000, A&A, 357, 219
Preibisch, Th. 1997, A&A, 320, 525
Preibisch, Th. 2003, A&A, 401, 543
Preibisch, Th., & Zinnecker, H. 2002, AJ, 123, 1613
Prusti, T., Whittet, D. C. B., & Wesselius, P. R. 1992, MNRAS, 254, 361
Raymond, J. C., & Smith, B. W. 1977, ApJS, 35, 419
Rieke, G. H., & Lebofsky, M. J. 1985, ApJ, 288, 618 (RL85)
Rutledge, R. E., Basri, G., Martín, E. L., & Bildsten, L. 2000, ApJ, 538, L141
Schmidt-Kaler, T. 1982, in Landolt-Börnstein, Group VI, ed. K.-H. Hellwege (Berlin: Springer), 2, 454
Schwartz, R. D. 1977, ApJS, 35, 161
Skinner, S. L., Güdel, M., Koyama, K., & Yamauchi, S. 1997, ApJ, 486, 886
Skinner, S. L., Brown, A., & Stewart, R. T. 1993, ApJS, 87, 217
Stelzer, B., & Huélamo, N. 2000, A&A, 363, 667
Stelzer, B., Neuhäuser, R., & Hambaryan, V. 2000, A&A, 356, 949
Strüder, L., Briel, U. G., Dennerl, K., et al. 2001, A&A, 365, L18
Takami, M., Bailey, J., & Chrysostomou, A. 2003, A&A, 397, 675
Tozzi, P., Rosati, P., Nonino, M., et al. 2001, ApJ, 562, 42
Tsuboi, Y., Koyama, K., Murakami, H., et al. 1998, ApJ, 503, 894
Turner, M. J. L., Abbey, A., Arnaud, M., et al. 2001, A&A, 365, L27
van den Ancker, M. E., de Winter, D., & Tjin A. Djie, H. R. E. 1998, A&A, 330, 145
Vuong, M. H., Montmerle, T., Grosso, N., et al. 2003, A&A, 408, 581
Walter, F. M. 1992, AJ, 104, 758
Whittet, D. C. B., Prusti, T., Franco, G. A. P., et al. 1997, A&A, 327, 1194
Wichmann, R., Krautter, J., Covino, E., et al. 1997, A&A, 320, 185
Wichmann, R., Bastian, U., Krautter, J., Jankovics, I., & Rucinski, S. M. 1998, MNRAS, 301, L39
Zapatero Osorio, M. R., Martín, E. L., & Rebolo, R. 1997, A&A, 323, 105
Zinnecker, H., & Preibisch, T. 1994, A&A, 292, 152

Online Material

Table 2. X-ray sources detected in the EPIC observation of Cha I at $ML > 20$. The columns denote X-ray source number, instrument by which the source was detected, X-ray position, maximum likelihood of source existence, number of broad band source counts, exposure time, hardness ratios, optical/IR counterpart, and distance between the X-ray source and the counterpart. For sources detected in the merged image we list the hardness ratios computed from the corresponding source found in pn, and no hardness ratio is computed if the source is detected only in the merged image.

Designation	Instr.	$\alpha_{x,2000}$	$\delta_{x,2000}$	ML	Cts	Exp. [s]	HR 1	HR 2	Identification	Δ_{ox} [″]
XMM-Cha I-1	ALL	11 04 32.7	–77 28 49.0	143.5	108.6 ± 10.4	31309.5	0.76 ± 0.11	−0.02 ± 0.20		
XMM-Cha I-2	ALL	11 04 42.4	–77 41 55.7	320.4	166.8 ± 12.9	42316.2	<−0.16	<−0.85	BYB 18	2.2
XMM-Cha I-3	M 2	11 05 03.6	–77 39 44.6	46.7	33.8 ± 5.8	49723.4	>0.84	0.16 ± 0.24	2M 110506-773944	1.4
XMM-Cha I-4	ALL	11 05 07.0	–77 33 42.9	21.3	37.4 ± 6.1	47340.8	–	–	2M 110507-773338	5.0
XMM-Cha I-5	ALL	11 05 09.3	–77 43 28.9	22.0	48.0 ± 6.9	44590.1	>0.82	0.01 ± 0.26		
XMM-Cha I-6	ALL	11 05 43.0	–77 26 50.6	1642.2	508.1 ± 22.5	34147.7	−0.28 ± 0.08	−0.93 ± 0.04	CHXR-15	1.9
XMM-Cha I-7	ALL	11 06 15.3	–77 37 50.3	265.8	194.4 ± 13.9	71956.2	0.45 ± 0.13	−0.65 ± 0.12	CCE 98-19	2.2
XMM-Cha I-8	ALL	11 06 15.7	–77 21 56.1	11306.0	2337.6 ± 48.3	14244.0	0.47 ± 0.03	−0.58 ± 0.03	Ced 110-IRS2	1.0
XMM-Cha I-9	ALL	11 06 28.8	–77 37 33.0	600.9	342.6 ± 18.5	75135.8	0.34 ± 0.10	−0.71 ± 0.09	CHXR-73	0.3
XMM-Cha I-10	M 2	11 06 44.5	–77 26 32.5	61.4	46.6 ± 6.8	38064.8	0.43 ± 0.18	−0.94 ± 0.07	UX Cha	3.3
XMM-Cha I-11	M 2	11 06 45.1	–77 27 00.7	562.5	180.7 ± 13.4	17263.0	0.70 ± 0.07	−0.69 ± 0.08	CHXR-20	2.8
XMM-Cha I-12	ALL	11 06 57.6	–77 42 10.1	3034.5	1037.6 ± 32.2	68823.7	0.11 ± 0.06	−0.80 ± 0.04	CHXR-74	0.8
XMM-Cha I-13	ALL	11 07 11.4	–77 46 37.2	2151.1	778.4 ± 27.9	47614.2	0.39 ± 0.07	−0.64 ± 0.06	CHXR-21	4.1
XMM-Cha I-14	M 1	11 07 12.1	–77 38 57.8	34.2	33.4 ± 5.8	38792.2	>0.84	0.33 ± 0.23		
XMM-Cha I-15	M 2	11 07 12.8	–77 43 48.2	310.7	151.4 ± 12.3	53775.0	0.39 ± 0.10	−0.61 ± 0.10	CHXR-22E/W	2.8/7.6
XMM-Cha I-16	PN	11 07 13.0	–77 23 06.9	34.9	35.8 ± 6.0	21981.5	>0.85	0.08 ± 0.24	CCE 98-23	11.6
XMM-Cha I-17	ALL	11 07 16.9	–77 35 52.3	66.2	79.8 ± 8.9	84142.5	−0.23 ± 0.18	−0.87 ± 0.13	ChaHα1	1.8
XMM-Cha I-18	ALL	11 07 19.5	–77 36 38.6	211.4	181.9 ± 13.5	85867.4	0.95 ± 0.04	0.46 ± 0.13		
XMM-Cha I-19	PN	11 07 20.6	–77 29 40.0	248.0	134.1 ± 11.6	39992.5	−0.61 ± 0.09	−0.87 ± 0.12	KG 2001-5	4.0
XMM-Cha I-20	M 2	11 07 20.7	–77 38 07.1	6182.4	1391.6 ± 37.3	66026.2	0.31 ± 0.04	−0.78 ± 0.03	LHα332-17	3.0
XMM-Cha I-21	M 1	11 07 32.9	–77 28 25.9	1289.1	362.1 ± 19.0	45877.1	−0.13 ± 0.07	−0.81 ± 0.06	CHXR-25	2.1
XMM-Cha I-22	ALL	11 07 35.1	–77 34 49.1	1997.0	849.7 ± 29.1	82940.4	0.13 ± 0.07	−0.90 ± 0.03	CHXR-76	2.0
XMM-Cha I-23	ALL	11 07 37.1	–77 33 33.2	6652.4	1980.5 ± 44.5	77381.9	0.62 ± 0.03	−0.58 ± 0.04	CHXR-26	0.4
XMM-Cha I-24	ALL	11 07 37.5	–77 47 14.3	107.7	94.7 ± 9.7	46535.7	−0.09 ± 0.20	−0.76 ± 0.18	KG 2001-19	5.5
XMM-Cha I-25	ALL	11 07 37.8	–77 35 29.1	68.9	83.1 ± 9.1	85628.3	<−0.33	<−0.64	ChaHα7	2.2
XMM-Cha I-26	ALL	11 07 43.1	–77 33 57.9	60.5	106.4 ± 10.3	79734.8	0.04 ± 0.19	−0.85 ± 0.13	ChaHα2	2.4
XMM-Cha I-27	M 2	11 07 43.3	–77 39 39.6	476.3	233.4 ± 15.3	37801.9	0.67 ± 0.06	−0.59 ± 0.08	HM 15	5.3
XMM-Cha I-28	ALL	11 07 46.1	–77 40 04.6	24.3	84.4 ± 9.2	81971.4	–	–	ChaHα8	6.5
XMM-Cha I-29	ALL	11 07 52.2	–77 36 57.4	279.0	229.3 ± 15.1	89429.2	0.10 ± 0.14	−1.00 ± 0.01	ChaHα3	3.5
XMM-Cha I-30	ALL	11 07 55.9	–77 27 24.5	12386.6	2842.1 ± 53.3	44689.5	0.34 ± 0.03	−0.72 ± 0.03	CHX-10a	3.6
XMM-Cha I-31	M 2	11 07 57.5	–77 38 44.7	238.0	260.3 ± 16.1	86223.8	0.84 ± 0.04	0.15 ± 0.09	HM 16	5.3
XMM-Cha I-32	ALL	11 08 01.5	–77 42 27.8	38290.7	8011.2 ± 89.5	71190.8	0.17 ± 0.02	−0.68 ± 0.02	VW Cha	1.6
XMM-Cha I-33	M 2	11 08 02.6	–77 38 42.1	968.0	330.6 ± 18.2	86564.1	0.95 ± 0.02	0.47 ± 0.07	CCE 98-32	5.4
XMM-Cha I-34	ALL	11 08 03.7	–77 39 13.1	116.0	171.4 ± 13.1	84836.8	0.68 ± 0.10	−0.28 ± 0.15	HD 97048	6.1
XMM-Cha I-35	ALL	11 08 11.2	–77 48 15.5	4170.3	1202.0 ± 34.7	41846.1	0.92 ± 0.02	0.05 ± 0.06	WGA J1108.1-7748	1.6
XMM-Cha I-36	M 1	11 08 13.0	–77 34 20.4	59.6	70.5 ± 8.4	81261.2	0.51 ± 0.14	−0.46 ± 0.17	2M 110813-773410	9.8
XMM-Cha I-37	M 2	11 08 14.7	–77 33 52.1	4941.1	1111.5 ± 33.3	39850.8	0.35 ± 0.04	−0.49 ± 0.04	Glass I	5.6
XMM-Cha I-38	ALL	11 08 15.8	–77 44 36.3	193.9	147.8 ± 12.2	55259.6	−0.26 ± 0.16	−0.40 ± 0.25	HM 19	3.5
XMM-Cha I-39	ALL	11 08 16.4	–77 44 09.9	50.0	63.0 ± 7.9	60469.5	−0.42 ± 0.18	−0.30 ± 0.36	ChaHα13	3.4
XMM-Cha I-40	ALL	11 08 19.3	–77 39 15.7	110.5	103.2 ± 10.2	83166.5	−0.05 ± 0.19	−0.95 ± 0.07	ChaHα4	5.3
XMM-Cha I-41	ALL	11 08 23.9	–77 41 45.3	80.1	109.2 ± 10.5	72702.2	<−0.30	<−0.65	ChaHα5	3.1
XMM-Cha I-42	PN	11 08 26.2	–77 34 20.6	20.7	51.1 ± 7.1	79942.4	0.52 ± 0.16	−0.20 ± 0.22	2M 110824-773422	5.7
XMM-Cha I-43	ALL	11 08 39.3	–77 34 18.0	40.0	70.8 ± 8.4	77325.5	<−0.42	<−0.48	ChaHα6	1.3
XMM-Cha I-44	ALL	11 08 45.1	–77 33 02.7	242.8	196.4 ± 14.0	70876.9	0.88 ± 0.06	−0.22 ± 0.14		
XMM-Cha I-45	PN	11 08 54.7	–77 32 09.6	120.9	93.0 ± 9.6	59275.0	−0.14 ± 0.14	−0.83 ± 0.11	CHXR-78	2.4
XMM-Cha I-46	ALL	11 09 07.1	–77 40 03.2	75.6	99.3 ± 10.0	71811.8	0.89 ± 0.08	0.35 ± 0.19		
XMM-Cha I-47	M 1	11 09 12.1	–77 29 11.3	6138.8	1163.0 ± 34.1	48242.7	−0.05 ± 0.04	−0.79 ± 0.03	Sz 30	1.0
XMM-Cha I-48	ALL	11 09 18.4	–77 47 37.9	1038.1	372.8 ± 19.3	33296.5	<−0.81	<−0.73	KG 2001-78	2.1
XMM-Cha I-49	ALL	11 09 20.1	–77 31 22.3	21.8	53.8 ± 7.3	57095.8	0.73 ± 0.20	0.73 ± 0.21		
XMM-Cha I-50	ALL	11 09 27.1	–77 25 29.0	20.0	32.3 ± 5.7	31772.6	–	–		
XMM-Cha I-51	ALL	11 09 45.5	–77 40 33.5	121.9	110.7 ± 10.5	60538.7	<−0.09	<−0.84	KG 2001-96	1.9
XMM-Cha I-52	ALL	11 09 47.9	–77 26 28.0	33.2	54.6 ± 7.4	34030.5	>0.74	−0.31 ± 0.30	KG 2001-101 = BYB 43	2.0
XMM-Cha I-53	ALL	11 09 57.6	–77 40 42.5	24.3	43.0 ± 6.6	56802.0	–	–	2M 110955-774045	7.6
XMM-Cha I-54	PN	11 09 58.9	–77 37 07.3	2343.6	1214.7 ± 34.9	57935.2	0.32 ± 0.04	−0.57 ± 0.04	WX Cha	1.6
XMM-Cha I-55	ALL	11 10 38.0	–77 32 39.2	2074.4	723.5 ± 26.9	44320.3	–	–	CHXR-47	4.9
XMM-Cha I-56	ALL	11 10 51.5	–77 43 10.9	80.6	81.3 ± 9.0	40649.2	0.75 ± 0.14	−0.31 ± 0.24		
XMM-Cha I-57	PN	11 10 55.0	–77 36 15.2	20.2	27.9 ± 5.3	45368.1	<−0.62	>−0.03		
XMM-Cha I-58	M 2	11 11 25.2	–77 41 50.0	21.4	22.7 ± 4.8	13717.4	0.50 ± 0.25	−0.72 ± 0.22		

BYB – Baud et al. (1984); 2 M – 2 MASS catalogue; CHXR – Feigelson et al. (1993); CCE 98 – Cambrésy et al. (1998); ChaHα – Comerón et al. (2000); KG 2001 – Kenyon & Gómez (2001); HM – Henize & Mendoza (1973); CHX – Feigelson & Kriss (1989); Sz – Schwartz (1977).

Table 3. Optical and IR properties for all Cha I members and candidate members in the *XMM-Newton* FOV. The Hα equivalent width ($W_{\mathrm{H}\alpha}$) is negative for emission. If more than one Hα measurement is available for a given star we list the maximum and the minimum value observed. The T Tauri type given in Col. 6 of the same table is assigned on the basis of $W_{\mathrm{H}\alpha}$ using the criteria put forth by Martín (1998). Columns 7 and 8 represent the extinction and magnitude used to derive L_{bol}; referring to the band given in Col. 9. The bolometric luminosity, effective temperature, age and mass have been computed as described in Sect. 3.3. L_{bol} has been calculated for $d = 160$ pc. We assign an age of 5×10^5 yr to objects on the birthline.

Designation	SpT	Ref.	$W_{\mathrm{H}\alpha}$ [Å]	Ref.	TTS	$A_{J/I}$ [mag]	J/I [mag]	Band	Ref.	$\log(L_{\mathrm{bol}}/L_\odot)$	$\log T_{\mathrm{eff}}$ [K]	Age [Myr]	Mass [$M_\odot$]
Spectroscopically confirmed Cha I members													
KG 2001-19	M 5	(1)	−7.3	(1)	W	0.3	12.24	*J*	(1)	−1.26	3.51	4.0	0.18
CHXR-21	K7	(2)	−8.0... + 1.0	(7)/(2)	C	1.0	11.11	*J*	(5)	−0.36	3.61	6.0	0.8
HM 19	M 3.5	(3)	−5.0... − 3.0	(3)/(7)	W	0.8	11.29	*J*	(5)	−0.63	3.54	2.0	0.3
VW Cha	M 0.5	(4)	−146.9... − 60.0	(3)/(7)	C	0.8	8.63	*J*	(5)	+0.52	3.59	<1.0	0.6
CHXR-74	M 4.5	(4)	−8.3... − 13.0	(8)/(4)	C	0.9	11.55	*J*	(5)	−0.72	3.53	1.5	0.25
BYB 18	M 4	(5)	–	–	W	0.5	11.80	*J*	(5)	−0.98	3.53	3.0	0.25
KG 2001-96	M 6.5	(1)	–	–	W	0.5	12.36	*J*	(1)	−1.24	3.48	≤2.0	0.11
HD 97048	A0	(3)	−30.0... − 37.0	(3)/(7)	–	0.4*	7.41	*J*	(3)	+1.58	4.02	2.0	2.5
CCE 98-19	M 2.5	(5)	–	–	W	2.9	12.59	*J*	(5)	−0.25	3.55	1.0	0.35
CHXR-73	M 4.5	(4)	–	–	W	1.8	12.60	*J*	(5)	−0.78	3.53	2.0	0.25
CHXR-76=BYB 34	M 5	(4)	−5.5... − 7.2	(4)/(8)	W	0.8	12.19	*J*	(5)	−1.04	3.51	2.5	0.18
CHXR-26	K7	(2)	–	–	W	2.3	11.41	*J*	(5)	+0.04	3.61	2.0	0.8
CHXR-47	K3	(2)	−0.4	(9)	W	1.4	8.45	*J*	(2)	+0.93	3.67	<0.5	1.5
CHX-10a	M 1	(2)	<−0.2	(10)	W	0.8	8.37	*J*	(2)	+0.61	3.57	<0.5	0.5
CHXR-15	M 5	(2)	−8.0	(9)	W	0.1	11.21	*J*	(2)	−0.93	3.51	2.0	0.18
KG 2001-101	M 1	(1)	−178	(1)	C	2.1	12.77	*J*	(1)	−0.63	3.57	4.0	0.5
Ced110-IRS2	G2	(3)	<−1.2	(3)	W	1.0*	7.64	*J*	(3)	+1.26	3.77	1.0	2.25
WX Cha	K7	(3)	−65.5... − 90.0	(3)/(7)	C	0.6*	10.00	*J*	(3)	−0.07	3.61	2.5	0.8
CHXR-78 C	M 5.5	(4)	−3.2... − 13.4	(4)/(8)	C	0.6	12.36	*J*	(5)	−1.19	3.51	3.0	0.18
CCE 98-23	M 1	(5)	–		C	8.6	17.55	*J*	(5),(11)	+0.06	3.57	<1.0	0.45
Sz 30	M 0	(3)	−5.2	(3)	W	0.3*	9.70	*J*	(3)/(12)	−0.11	3.59	1.5	0.6
CHXR-25	M 4	(2)	1.2	(2)	W	0.0	11.69	*J*	(2)	−1.14	3.53	5.0	0.25
CHXR-22 E	M 3	(2)	–	–	W	1.8	10.18	*J*	(2)	+0.22	3.54	0.5	0.3
CHXR-22 W	K7	(2)	–	–	W	1.9	12.56	*J*	(2)	−0.58	3.61	10.0	0.8
HM 15	M 1	(4)	−47.9... − 70.0	(3)/(4)	C	1.3	10.22	*J*	(5)	+0.07	3.57	<1.0	0.5
CCE 98-32	M 2	(5)	–	–	C	3.4	11.51	*J*	(5)	+0.39	3.55	0.5	0.35
HM 16	K7	(4)	−61.0... − 75.0	(4)/(7)	C	2.3	9.71	*J*	(5)	+0.72	3.61	<0.5	0.8
LHα332-17	G2	(3)	−17.2	(3)	C	1.2	7.99	*J*	(5)	+1.20	3.77	1.5	2.4
Glass I	K7	(4)	−4.0... − 11.0	(3)/(4)	W	1.5	8.58	*J*	(5)	+0.86	3.61	<0.5	0.8
CHXR-20	M 0	(2)	0.1	(2)	W	0.6	9.88	*J*	(2)	−0.06	3.59	1.0	0.6
ChaHα1	M 7.5	(6)	−34.5... − 59.0	(8)/(4)	C	0.11	16.17	*I*	(6)	−1.95	3.46	5.0	0.06
ChaHα2	M 6.5	(6)	−39.0... − 71.0	(6)/(8)	C	0.40	15.08	*I*	(6)	−1.58	3.48	4.0	0.09
ChaHα3	M 7	(6)	−4.5... − 14.4	(6)/(8)	W	0.16	14.89	*I*	(6)	−1.45	3.46	≤1.6	0.07
ChaHα4	M 6	(6)	−4.7... − 9.7	(4)/(8)	W	0.29	14.34	*I*	(6)	−1.33	3.48	2.5	0.10
ChaHα5	M 6	(6)	−7.6... − 8.0	(4)/(8)	W	0.47	14.68	*I*	(6)	−1.40	3.48	3.2	0.10
ChaHα6	M 7	(6)	−59.0... − 61.7	(6)/(8)	C	0.13	15.13	*I*	(6)	−1.56	3.46	1.6	0.06
ChaHα7	M 8	(6)	−35.0... − 45.0	(8)/(6)	C	0.14	16.86	*I*	(6)	−2.18	3.44	6.3	0.04
ChaHα8	M 6.5	(6)	−8.4... − 9.0	(8)/(6)	W	0.34	15.47	*I*	(6)	−1.76	3.48	5.0	0.10
ChaHα9	M 6	(6)	−16.0	(6)	W	0.76	17.34	*I*	(6)	−2.34	3.48	30.0	0.09
ChaHα10	M 7.5	(6)	−9.0	(6)	W	0.05	16.90	*I*	(6)	−2.27	3.46	12.0	0.06
ChaHα11	M 8	(6)	−23.0	(6)	C	0.0	17.35	*I*	(6)	−2.44	3.44	12.0	0.04
ChaHα12	M 7	(6)	−20.0	(6)	C	0.5 :	15.58	*I*	(6)	−1.59	3.46	1.6	0.06
ChaHα13	M 5	(6)	−11.0	(6)	W	0.89	14.09	*I*	(6)	−1.06	3.51	2.0	0.18
IR Nebula	M 5	(5)	–	–		3.2	11.12	*J*	(5)	+0.34	3.51	<0.5	0.18
Photometric Cha I candidates													
UX Cha	M 1.5		<−5.0	(7)	W	0.9	10.81	*J*	2 MASS	−0.32	3.57	2.0	0.4
KG 2001-78	A2		–	–		0.8	7.73	*J*	2 MASS	+1.53	3.95	4.0	2.0
KG 2001-5	M 1		–	–		0.2	11.31	*J*	(12)	−0.80	3.57	3.0	0.45
2M 110955-774045	M 1		–	–		1.5	15.90	*J*	2 MASS	−2.12	3.57		
2M 110507-773338	M 3		–	–		1.2	15.96	*J*	2 MASS	−2.34	3.54		
2M 110824-773422	M 0.5		–	–		0.8	14.37	*J*	2 MASS	−1.78	3.59		
2M 110813-773410	M 2		–	–		0.9	16.24	*J*	2 MASS	−2.51	3.55		
2M 110506-773944	M 0		–	–		2.3	13.29	*J*	2 MASS	−0.74	3.59	8.0	0.6

* A_J calculated from the literature values for A_{V} using the RL85-extinction law.

(1) – Comerón et al. (2004); (2) – Lawson et al. (1996); (3) – Gauvin & Strom (1992); (4) – Comerón et al. (1999); (5) – Gómez & Mardones (2003); (6) – Comerón et al. (2000); (7) – Hartigan (1993); (8) – Hartigan (1993); (9) – Neuhäuser et al. (1999); (10) – Walter (1992); (11) – Cambrésy et al. (1998); (12) – Kenyon & Gómez (2001).

Table 4. Spectral parameters of bright X-ray sources in the Cha I *XMM-Newton* field. The columns represent: source number, identification, number of counts in the background-subtracted spectrum, reduced χ^2 of best fit, absorbing hydrogen column density derived from A_J using the relation by Paresce et al. (1984) and held fixed during the fitting process, X-ray temperature(s) of 2-component thermal MEKAL model, and emission measures of each temperature component assuming a distance of 160 pc.

Source	Ident.	Net counts	$\chi^2_{\rm red}$ (d.o.f.)	$N_{\rm H}$	kT_1	kT_2	$\log EM_1$	$\log EM_2$
				[10^{22} cm^{-2}]	[keV]	[keV]	[erg/cm^2/s]	[erg/cm^2/s]
XMM-Cha I-2	BYB 18	92	1.13 (6)	=0.31	0.21	1.01	52.21	52.10
XMM-Cha I-6	CHXR-15	264	1.00 (16)	=0.06	0.34	1.12	51.89	52.46
XMM-Cha I-7	CCE 98-19	77	1.36 (3)	=1.82	0.22	79.2	54.24	51.82
XMM-Cha I-8	Ced 110 IRS-2	2454	1.27 (72)	=0.60	0.66	2.15	53.80	53.89
XMM-Cha I-9	CHXR-73	235	1.29 (6)	=1.13	0.22	0.86	53.52	52.75
XMM-Cha I-11	CHXR-20	132	1.43 (11)	=0.38	0.33	1.72	52.41	52.87
XMM-Cha I-12	CHXR-74	457	1.20 (22)	=0.57	0.25	1.24	53.31	52.74
XMM-Cha I-13	CHXR-21	107	1.26 (9)	=0.63	0.11	1.27	54.72	52.57
XMM-Cha I-15	CHXR-22	125	1.21 (15)	=1.20	0.20	1.39	54.15	52.71
XMM-Cha I-20	LHα332-17	1165	1.40 (70)	=0.75	0.27	1.03	54.11	53.42
XMM-Cha I-21	CHXR-25	369	0.94 (16)	=0.00	0.51	1.79	52.43	52.61
XMM-Cha I-22	CHXR-76	352	0.96 (19)	=0.50	0.54	1.00	52.54	52.52
XMM-Cha I-23	CHXR-26	401	0.57 (22)	=1.45	0.26	1.76	54.31	52.94
XMM-Cha I-27	HM 15	166	1.27 (11)	=0.82	0.22	1.72	53.49	52.76
XMM-Cha I-29	ChaHα3	110	0.99 (9)	=0.35	0.59	1.16	51.49	51.97
XMM-Cha I-30	CHX-10a	1327	0.88 (47)	=0.47	0.61	1.42	53.07	53.38
XMM-Cha I-31	HM 16	99	1.19 (8)	=1.45	0.18	6.40	54.12	52.62
XMM-Cha I-32	VW Cha	3328	1.29 (93)	=0.50	0.32	1.57	53.80	53.58
XMM-Cha I-33	CCE 98-32	92	0.66 (7)	=2.14	0.25	17.93	53.99	52.82
XMM-Cha I-34	HD 97048	74	1.58 (6)	=0.23	0.19	79.90	52.70	51.98
XMM-Cha I-37	Glass I	784	1.37 (47)	=0.94	0.19	3.61	54.99	53.10
XMM-Cha I-47	Sz 30	1036	1.29 (64)	=0.21	0.32	1.24	53.41	53.30
XMM-Cha I-48	KG 2001-78	190	1.27 (12)	=0.50	0.08	0.20	54.62	53.59
XMM-Cha I-54	WX Cha	905	1.35 (33)	=0.37	0.62	2.28	52.75	52.95
XMM-Cha I-55	CHXR-47	357	0.99 (24)	=0.88	0.17	1.39	54.06	53.11

Table 5. X-ray luminosities in the 0.4−2.5 keV band for d = 160 pc, X-ray to bolometric luminosity ratio, and probability for variability of the source according to the KS-test. The flag in Col. 3 indicates the method used to derive L_x: "S" – spectral fit with 2-T model and column density fixed to the value expected for the galactic $N_H - A_V$ relation; "L" – absorption from the literature and $\log T$ [K] = 6.95; "N" – absorption newly derived in this paper from *JHK* colors and $\log T$ [K] = 6.95.

Designation	$\log L_x$ [erg/s]	Flag L_x	$\log (L_x/L_{bol})$	KS prob.
Spectroscopically confirmed Cha I members				
KG 2001-19	28.67	L	−3.66	–
CHXR-21	30.83	S	−2.40	95%
HM 19	29.44	L	−3.52	–
VW Cha	30.97	S	−3.13	100%
CHXR-74	30.30	S	−2.57	–
BYB 18	29.36	S	−3.25	100%
KG 2001-96	28.90	L	−3.45	–
HD 97048	29.58	S	−5.72	–
CCE 98-19	30.92	S	−2.41	–
CHXR-73	30.49	S	−2.31	100%
CHXR-76	29.92	S	−2.62	–
CHXR-26	31.27	S	−2.35	100%
CHXR-47	30.77	S	−3.75	–
CHX-10a	30.56	S	−3.64	99%
CHXR-15	29.56	S	−3.10	–
BYB 43	29.08	L	−3.88	100%
Ced 110 IRS-2	31.16	S	−3.69	100%
WX Cha	30.17	S	−3.35	–
CHXR-78 C	28.96	L	−3.44	–
CCE 98-23	30.33	L	−3.32	–
Sz 30	30.62	S	−2.86	99%
CHXR-25	29.82	S	−2.63	97%
CHXR-22 E	30.94	S	−2.87	–
HM 15	30.47	S	−3.18	–
CCE 98-32	31.06	S	−2.92	100%
HM 16	31.00	S	−3.31	–
LHα332-17	31.09	S	−3.70	97%
Glass I	31.79	S	−2.65	–
CHXR-20	30.03	S	−3.49	–
ChaHα1	28.25	L	−3.39	–
ChaHα2	28.49	L	−3.52	–
ChaHα3	29.11	S	−3.03	–
ChaHα4	28.41	L	−3.85	–
ChaHα5	29.21	L	−2.98	–
ChaHα6	28.91	L	−3.12	–
ChaHα7	28.27	L	−3.14	–
ChaHα8	28.44	L	−3.39	99%
ChaHα9	<27.92	L	<−3.33	–
ChaHα10	<27.78	L	<−3.54	–
ChaHα11	<27.67	L	<−3.48	–
ChaHα12	<28.19	L	<−3.81	–
ChaHα13	29.02	L	−3.51	97%
IR Nebula	<29.16	L	<−4.77	–
Photometric candidates				
UX Cha	29.53	N	−3.74	–
KG 2001-78	30.56	S	−4.56	–
KG 2001-5	28.86	L	−3.93	–
2M 110506-773944	29.51	N	−3.34	–